DISSERTATION

PET/CT and SPECT/CT for monitoring treatment response and treatment related morbidities in various oncological and non-oncological rodent models

PET/CT und SPECT/CT zur Erfassung des Therapieansprechens sowie von therapiebedingten Veränderungen in verschiedenen onkologischen und nicht-onkologischen Nagetiermodellen

zur Erlangung des akademischen Grades
Doctor of Philosophy (PhD)

vorgelegt der Medizinischen Fakultät
Charité – Universitätsmedizin Berlin

von

Ajay Mohan Mohan

Erstbetreuung: Professor Dr. med. Winfried Brenner

Datum der Promotion: 29 November 2024

Table of contents

List of tables

List of figures

List of abbreviations

AKI	Acute Kidney Injury
ANOVA	Analysis of Variance
BERIC	Berlin Experimental Radionuclide Imaging Center
CT	Computed Tomography
DMEM	Dulbecco’s Modified Eagle Medium
DOTA	1,4,7,10-tetraazacyclododecane-1,4,7,10-tetraaceticacid
DPD	Diphosphono-1,2-Propan-Dicarbon
DTC	Differentiated Thyroid Cancer
ENETS	European Neuroendocrine Tumor Society
FCS	Fetal Calf Serum
^{18}F-FDG	^{18}Fluorine-Fluorodeoxyglucose
^{68}Ga	^{68}Gallium
GEP	Gastroenteropancreatic
HDP	Hydroxymethylene Diphosphonate
HE	Hematoxylin Eosin
IHC	Immunohistochemistry
^{111}In	^{111}Indium
I	Iodine
JR11	Satoreotide tetraxetan
^{177}Lu	^{177}Lutetium
MAG3	Mercaptoacetyltriglycine
MDP	Methylene Diphosphonate
MRI	Magnetic Resonance Imaging
mTORC1	Mammalian Target Of Rapamycin Complex 1
MWU	Mann Whitney U

$NaTcO_4^-$	Sodium Pertechnetate
NEC	Neuroendocrine Carcinoma
NET	Neuroendocrine Tumor
NOC	NaI^3-Octreotide
OAT	Organic Anion Transporters
OTM	Orthodontic Tooth Movement
PET	Positron Emission Tomography
PI3K	Phosphatidiylinositol 3 Kinase
PRRT	Peptide Receptor Radionuclide Therapy
SCID	Severe Combined Immuno Deficient
SSA	Somatostatin Analogues
SSTR	Somatostatin Receptor
SPECT	Single Photon Emission Computed Tomography
SPSS	Statistical Package for Social Sciences
SUV	Standardized Uptake Value
TAC	Time Activity Curves
TATE	Tyr^3-Octreotate
^{99m}Tc	^{99m}Technetium
T_{max}	Time to maximum uptake
TOC	Phe^1-Tyr^3-Octreotide
T_{50}	Time to 50% clearance
T_{25}	Time to 75% clearance
VOI	Volume of Interest
WHO	World Health Organisation
3R	Reduce, Refine, Replace

Abstract

Aim

Quantitative radionuclide imaging using PET and SPECT with different radiopharmaceuticals is a mainstay in functional imaging, therapy response monitoring and characterization of treatment-induced changes and morbidities. The overall goal of this thesis was to translate clinically well-established PET and SPECT procedures into experimental preclinical settings to improve and extend the in-vivo characterization of treatment-related changes in various interventional animal models.

Materials and Methods

For overcoming everolimus resistance in neuroendocrine tumors (NET), a novel treatment approach with the PI3Kα inhibitor alpelisib was evaluated in a SCID mouse model with everolimus resistant and wildtype NET tumors using PET with ^{18}F-FDG and ^{68}Ga-DOTATOC as in-vivo measures for longitudinal assessment of tumor response and somatostatin receptor (SSTR) (re-)expression. Furthermore, the renal toxicity of the different treatment regimens with alpelisib as well as ^{177}lutetium SSTR ligand therapies was evaluated in NET tumor-bearing SCID mice by renal SPECT with ^{99m}Tc-MAG3 after normal tracer kinetic values have been established in healthy male and female SCID mice. Finally, bone remodelling after piezocision for orthodontic applications in rats was monitored by bone SPECT imaging with ^{99m}Tc-MDP as a marker for bone metabolism before and 2 and 4 weeks after treatment.

Results

In everolimus sensitive tumors, everolimus, alpelisib, and the combination treatment significantly prolonged survival compared to placebo, while in everolimus resistant tumors only the combination therapy had a significant effect. PET imaging showed negative ^{68}Ga-DOTATOC and positive ^{18}F-FDG tumor uptake throughout the entire treatment period in all treatment groups, indicating no SSTR re-expression, as validated by histological analysis.

Normal renal function values in male and female mice showed that males had significantly delayed T_{25} clearance ($p < 0.01$). After treatment with ^{177}lutetium SSTR ligands, time activity curves exhibited a less steep slope indicating a delayed clearance reaching T_{50} ($p = 0.02$) and T_{25} ($p = 0.01$) later compared to healthy mice. Alpelisib also significantly delayed T_{50} and T_{25} ($p = 0.013$ each) compared to pretreatment.

Bone SPECT was highly sensitive in detecting bone remodelling after surgery demonstrating an increased uptake at 2 weeks ($p = 0.001$) which gradually decreased at 4 weeks after orthodontic appliance application with/without piezocision. However, no additional significant effect of piezocision on bone metabolism was observed.

Conclusion

With respect to the overall goal of translating and implementing dedicated radionuclide imaging procedures with SPECT and PET in preclinical animal research, imaging protocols were established and validated as a basis for improved monitoring of treatment response and treatment-related morbidities in various oncological and non-oncological rodent models.

Zusammenfassung

Ziel

Die quantitative Radionuklid-Bildgebung mit PET und SPECT mit verschiedenen Radiopharmaka ist eine wichtige Grundlage für die funktionelle Bildgebung zur Überwachung des Therapieansprechens und der Charakterisierung von behandlungsbedingten Veränderungen. Das übergeordnete Ziel dieser Arbeit war es, klinisch etablierte PET und SPECT Verfahren in die präklinische Anwendung zu übertragen, um die in vivo-Charakterisierung von behandlungsbedingten Veränderungen in verschiedenen Tiermodellen zu verbessern und zu erweitern.

Material und Methoden

Zur Überwindung der Everolimus Resistenz bei neuroendokrinen Tumoren (NET) wurde ein neuartiger Behandlungsansatz mit dem PI3Kα-Inhibitor Alpelisib in einem SCID-Mausmodell mit Everolimus-resistenten und Wildtyp NET-Tumoren untersucht und mit Hilfe von ^{18}F-FDG und ^{68}Ga-DOTATOC PET das Tumoransprechen und die Somatostatin-Rezeptor (Re-) Expression (SSTR) im Verlauf evaluiert.

Darüber hinaus wurde die Nierentoxizität der verschiedenen Behandlungsschemata mit Alpelisib sowie bei der ^{177}Lutetium-SSTR-Ligandentherapie in SCID-Mäusen mittels Nieren-SPECT mit ^{99m}Tc-MAG3 untersucht, nachdem Normalwerte für die Biokinetik des Tracers in gesunden männlichen und weiblichen SCID-Mäusen bestimmt worden waren. Schließlich wurde der Knochenumbau nach Piezozision im Rahmen von kieferorthopädi-

sche Eingriffen bei Ratten mittels Knochen-SPECT-Bildgebung mit ^{99m}Tc-MDP als Marker für den Knochenstoffwechsel vor sowie 2 und 4 Wochen nach der Behandlung bestimmt.

Ergebnisse

Bei Everolimus-sensitiven Tumoren verlängerten Everolimus, Alpelisib und die Kombinationstherapie das Überleben im Vergleich zu Placebo signifikant, während bei Everolimus-resistenten Tumoren nur die Kombinationstherapie das Überleben signifikant verlängerte. Die PET-Bildgebung zeigte während des gesamten Behandlungszeitraums in allen Behandlungsgruppen eine fehlende ^{68}Ga-DOTATOC- und eine positive ^{18}F-FDG-Tumoraufnahme. Dies deutet darauf hin, dass keine Redifferenzierung von SSTR stattgefunden hat, was die histologische Analyse bestätigte.

Normale Nierenfunktionswerte bei männlichen und weiblichen Mäusen zeigten, dass die Männchen eine deutlich verzögerte T_{25}-Clearance hatten ($p < 0,01$). Nach der Behandlung mit ^{177}Lutetium-SSTR-Liganden wiesen die Zeit-Aktivitäts-Kurven einen weniger steilen Abfall mit einer verzögerten T_{50} ($p = 0,02$) und T_{25} ($p = 0,01$) Clearance auf im Vergleich zu gesunden Mäusen. Auch Alpelisib verzögerte T_{50} und T_{25} (jeweils $p = 0,013$) im Vergleich zu den prätherapeutischen Werten signifikant.

Die Knochen-SPECT war sehr empfindlich beim Nachweis des gesteigerten Knochenumbaus nach Operation und zeigte eine erhöhte Traceraufnahme nach 2 Wochen ($p = 0,001$), die 4 Wochen nach Einbau der kieferorthopädischen Apparatur mit/ohne Piezozision allmählich abnahm. Es wurde jedoch kein zusätzlicher signifikanter Effekt der Piezozision auf den Knochenstoffwechsel beobachtet.

Fazit

Im Hinblick auf das übergeordnete Ziel, verschiedene Radionuklid-Bildgebungsverfahren mit SPECT und PET in die präklinischen Tierforschung zu übertragen, wurden Bildgebungsprotokolle als Grundlage für eine verbesserte in vivo Überwachung des Therapieansprechens und von behandlungsbedingten Morbiditäten in verschiedenen onkologischen und nicht-onkologischen Nagetiermodellen erstellt und validiert.

1 Introduction

Nuclear medicine and radionuclide imaging methods such as single photon emission computed tomography (SPECT) and positron emission tomography (PET), often combined with computed tomography (CT), in combination with a variety of organ or disease specific tracers have become a mainstay in functional tumor imaging as well as response monitoring and characterization of treatment-induced changes in tumor phenotype. As radionuclide imaging with SPECT/CT and PET/CT is a basic tool for quantitative imaging of organ, cellular and molecular function such as kidney function, state of (e.g. bone, tumor) metabolism, or receptor expression, SPECT and PET can be also applied for characterization of treatment-related non-tumor alterations, e.g. kidney toxicity in tumor therapy, or bone remodelling after surgical interventions.

1.1 Research Objectives

The overarching goal of this thesis was to translate clinically well-established PET and SPECT imaging procedures into experimental preclinical settings to improve and expand the non-invasive in-vivo characterization possibilities of treatment-induced changes in various interventional animal models and, thus, help generating longitudinal data in animals, in analogy to patients, which cannot be produced by standard animal experiments which primarily rely on histopathological data at one time point per animal only.

In a first comprehensive study on everolimus resistance in neuroendocrine tumors (NET), a new treatment approach with the PI3Kα inhibitor alpelisib was evaluated in a xenograft mouse tumor model with everolimus resistant and wildtype NET cells using PET with ^{18}fluorine-fluorodeoxyglucose (^{18}F-FDG) and ^{68}gallium-1,4,7,10-tetraazacyclododecane-1,4,7,10-tetraaceticacid- Phe^{1}-Tyr^{3}-Octreotide (^{68}Ga-DOTATOC) as non-invasive in-vivo readouts for longitudinal tumor response assessment and somatostatin receptor (SSTR) (re-)expression.

In a second study, the treatment-related kidney toxicity of the various treatment regimens with alpelisib as well as of ^{177}lutetium (^{177}Lu) somatostatin receptor (SSTR) ligand therapies in NET tumor-bearing severe combined immune deficient (SCID) mice was evaluated by renal SPECT with ^{99m}Technetium-mercaptoacetyltriglycine (^{99m}Tc-MAG3) after establishing normal tracer kinetic uptake values in both healthy male and female SCID mice.

In a third study, bone remodelling after piezocision for orthodontic applications was monitored in rats by bone SPECT/CT imaging with ^{99m}Tc-methylene diphosphonate (^{99m}Tc-MDP) as a marker for bone metabolism before and after treatment.

1.2 Imaging and treatment of Neuroendocrine Tumors

Neuroendocrine tumors are tumors arising from both a neural and endocrine origin. NET can be broadly classified based on their somatostatin receptor expression on the tumor surface as well-differentiated (high SSTR expression), moderately differentiated (low-high SSTR) and poorly differentiated (very low-nil SSTR) tumors. NET are graded based on morphology and Ki-67 proliferation index as Grade 1 (G1, well differentiated, Ki-67 ≤2%), G2 (moderately differentiated, Ki-67 3-20%) and G3 (poorly differentiated, Ki-67 >20%) tumors (Popa et al., 2021). Somatostatin receptors are members of the G protein coupled receptor family, and are overexpressed in G1 and G2 NET. There are five different types of SSTRs namely SSTR1, SSTR2… SSTR5, of which SSTR2 has the most predominant expression in most of the neuroendocrine tumors. The most commonly used PET agonist somatostatin analogues (SSA) are Phe^{1}-Tyr^{3}-Octreotide (TOC), Nal^{3}-Octreotide (NOC), and Tyr^{3}-Octreotate (TATE) coupled to ^{68}Ga through the 1,4,7,10-tetraazacyclododecane-1,4,7,10-tetraaceticacid (DOTA) chelator. These different analogues are synthesized by modification of various amino acid sequences and accordingly they have specific receptor affinities. The specific amino acid sequences of various somatostatin analogues and the corresponding receptor affinities are summarized in Table 1.

Table 1: Somatostatin Analogues Sequences

Respective somatostatin receptor affinity and amino acid sequences of different somatostatin agonist analogues.

Amino Acid Sequence	Hormone Analogue	SSTR affinity
Ala-Gly-Cys-Lys-Asn-Phe-Phe-Try-Lys-Thr-Phe-Thr-Ser-Cys	Somatostatin	
DOTA-D-Phe-Cys-Tyr-D-Trp-Lys-Thr-Cys-Thr(ol)	DOTA-TOC	SSTR2, SSTR5
DOTA-D-Phe-Cys-Nal-D-Trp-Lys-Thr-Cys-Thr(ol)	DOTA-NOC	SSTR3, SSTR5
DOTA-D-Phe-Cys-Tyr-D-Trp-Lys-Thr-Cys-Thr(OH)	DOTA-TATE	SSTR2

from Mohan et al. (Mohan et al., 2021)

Studies on positron emission tomography/computed tomography (PET/CT) with somatostatin analogues have reported sensitivities of 88-93% and specificities of 88-95% for the detection of well-differentiated NET (Treglia et al., 2012, Yang et al., 2014). The joint guidelines of the American Society and the European Association of Nuclear Medicine recommend the use of ^{18}F-FDG and ^{68}Ga-DOTATOC for identification of poorly differentiated, and well and moderately differentiated lesions, respectively (Hope et al., 2023). For dual PET imaging with both ^{18}F-FDG and ^{68}Ga-DOTATOC, a higher prognostic value for the management of both well and poorly differentiated NET was found (Chen et al., 2018, Hindie, 2017, Kumar et al., 2011, Naswa et al., 2010) showing a sensitivity and specificity of 49% and 73%, respectively, in delineating the different grades of NET (Kayani et al., 2008, Paiella et al., 2021, Panagiotidis et al., 2017, Zhang et al., 2018, Zhou et al., 2021).

NET arising from the pancreas namely pancreatic neuroendocrine tumors (panNET) are a rare entity with an incidence of 1/100,000, steadily increasing in number every year (Akirov et al., 2019, Kelgiorgi and Dervenis, 2017). They are aggressive in nature characterized by slow indolent tumor growth but high tumor grade, and usually manifest with lymph node, liver and distant metastases at the time of initial diagnosis and, thus, reduced survival (Kelgiorgi and Dervenis, 2017, Megdanova-Chipeva et al., 2020, Ro et al., 2013). The major treatment strategies for panNET include surgery, radiation therapy, molecular targeted therapy, somatostatin analogue therapy, peptide receptor radionuclide therapy (PRRT), and liver directed therapies (Akirov et al., 2019). PRRT is a type of targeted radionuclide therapy involving systematic administration of somatostatin analogues labelled to therapeutic radionuclides. These radiolabelled SSA are either internalized or bind to SSTRs thereby irradiating the cancer cells. Of all the different available therapeutic SSAs, ^{177}lutetium (^{177}Lu) labelled DOTATATE exhibited promising results and therapeutic efficacy. It was also shown that although all ^{177}Lu labelled agonist analogues namely DOTATOC, DOTANOC and DOTATATE have a similar biodistribution in normal organs (e.g. liver, kidney), ^{177}Lu-DOTATATE has a 3-4 fold higher tumor uptake and a lower whole-body retention making it the treatment of choice in NET patients (Kwekkeboom et al., 2001, Kam et al., 2012). This was further proved by the NETTER trial wherein ^{177}Lu-DOTATATE treatment in patients with midgut tumors resulted in significantly longer progression-free survival (Strosberg et al., 2017, Strosberg et al., 2021). This led to the approval of ^{177}Lu-DOTATATE for the treatment of gastroenteropancreatic (GEP) NET by

the US Food and Drug Administration (FDA) in 2018 (Hope et al., 2022). Since then PRRT has become the standard of care in well differentiated SSTR expressing metastasized neuroendocrine tumors. Moreover, PRRT is applied as a neoadjuvant therapy regimen in case of unresectable NET (Parghane et al., 2021). The success of PRRT could not be extrapolated to G3 NETs owing to their nil to negligible SSTR expression. For advanced G3 panNET, everolimus, a mTOR complex1 (mTORC1) inhibitor, was approved for systemic molecular targeted therapy in 2011 as these tumors depict an increased activation of phosphatidylinositol-3-kinase (PI3K)/Akt and mammalian target of rapamycin (mTOR) signaling pathway promoting tumor growth (Ciołczyk-Wierzbicka et al., 2020, Chan et al., 2017b, Pavel and Sers, 2016, Lee et al., 2018).

1.3 Everolimus Resistance in advanced panNET

The latest European Neuroendocrine Society (ENETS) guidelines recommend the use of everolimus as a second line of therapy following SSA treatment (Del Rivero et al., 2023, Pavel et al., 2016). The guidelines also suggest that everolimus be used as first line of therapy in cases of SSA therapy failure or infeasibility of systemic chemotherapy (Pavel and de Herder, 2017, Pavel et al., 2016). Thus, everolimus gained widespread significance owing to its significant clinical benefit as evidenced by the RADIANT-3 trial in advanced panNET patients (Lee et al., 2018, Yao et al., 2016). However, following initial disease stabilisation, patients under everolimus treatment often develop resistance within 1 year with tumor progression and metastases formation. Results from various preclinical studies attribute the resistance to mTOR inhibitors to over-activation of various associated signaling pathways (Curigliano et al., 2021). Recently, Santoni et al. described the different mutations and the cross talk happening between the mTORC1 and PI3K/Akt pathways in the development of everolimus resistance (Santoni et al., 2014).

Phosphatidylinositol-3-kinase is the commonly activated pathway in most cancers by regulating cell survival, proliferation and differentiation (Liu et al., 2009). Since then many PI3K pathway inhibitors have been developed and assessed for their chemotherapeutic efficacy in the treatment of various cancer entities. Among the various PI3K inhibitors, alpelisib, an isoform of PI3K-Akt pathway (PI3Kα) inhibitor, exhibited significant antitumor activity in various tumor xenograft models (Fritsch et al., 2014, Elkabets et al., 2013). In a phase-I clinical trial on breast cancer patients, alpelisib exhibited anti-tumor effects in 44% of tumors with PI3K mutation and 20% in wild type tumors (Mayer et al., 2017).

Various in-vitro studies conducted on different NET cell lines clearly indicate the potential of synergistic application of alpelisib and everolimus in overcoming resistance towards everolimus (Nölting et al., 2017). Similarly, studies have also reported the concomitant therapeutic efficacy of alpelisib and everolimus in two everolimus resistant cell lines, namely BON1 RR1 and BON1 RR2 (Aristizabal Prada et al., 2018). Additionally, Prada et al. described that a dual targeting approach in overcoming everolimus resistance resulted in the re-expression of SSTR in tumors which would make PRRT a therapeutic option even in tumors with initially low to nil SSTR expression (Aristizabal Prada et al., 2018).

In the present work, treatment with alpelisib was evaluated in an orthotopic xenograft SCID mouse tumor model with everolimus-resistant and wildtype NET cells using PET with ^{18}F-FDG and ^{68}Ga-DOTATOC as readouts for longitudinal tumor response assessment and somatostatin receptor (re-)expression.

1.4 Renal toxicity associated with PRRT and chemotherapy

Acute kidney injury (AKI) is one of the major toxic side effect of various drugs used for anti-tumoral therapy (Rosner and Perazella, 2019). Renal toxicity associated with chemotherapy, on the one hand restricts the effectiveness of the treatment, and on the other hand, it also affects the patient's quality of life. The same is true for radionuclide therapy with ^{177}Lu-DOTATATE and other ^{177}Lu-labelled SSTR analogues, in which the kidneys, besides bone marrow, are the critical organ in patients undergoing PRRT (Alsadik et al., 2022, Zhang et al., 2019). Renal scintigraphy with ^{99m}technetium-mercaptoacetyltriglycine (^{99m}Tc-MAG3) is the most widely used scintigraphic methodology in the assessment of renal function in various pathological conditions (Eshima and Taylor, 1992). ^{99m}Tc-MAG3 is a tubular agent that is actively taken out of the renal blood flow through the basolateral membrane mediated by organic anion transporters (OAT) expressed in the proximal tubules of the nephron (Benzakoun et al., 2020). Thus, side-related renal function and its potential impairment due to anti-tumor treatment can be quantified based on the excretion of ^{99m}Tc-MAG3 from the kidneys in terms of renal time-to-peak (T_{max}), T_{50} (50% clearance) and T_{25} (75% clearance).

In the present work, age- and sex-related normal kidney uptake parameters in both healthy male and female SCID mice were established for ^{99m}Tc-MAG3 SPECT imaging,

and subsequently kidney toxicity of ^{177}Lu-DOTATOC and ^{177}Lu-DOTA-JR11 was evaluated in NET tumor-bearing SCID mice by renal SPECT. Furthermore, kidney toxicity of the various treatment combinations of alpelisib and everolimus was investigated as well.

1.5 Bone remodelling after bone directed treatments

Bone remodelling is a complex process involving the osteocytes, osteoblasts and osteoclasts which ultimately protects the structural integrity and function of a specific bone (Rowe et al., 2023). It mainly constitutes the resorption of old or damaged areas of the bone by the osteoclasts and deposition of new matrix material namely the hydroxyapatite crystals by the osteoblasts (Rowe et al., 2023). ^{99m}Tc-labelled bisphosphonate compounds such as methylene diphosphonate (^{99m}Tc-MDP), hydroxymethylene diphosphonate (^{99m}Tc-HDP) and diphosphono-1,2-propan-dicarbon acid (^{99m}Tc-DPD) get attached to the surface of hydroxyapatite crystals, and are widely used for SPECT imaging of the skeletal system. The uptake of the tracer is proportional to the local osteoblastic matrix production, which is upregulated in various pathological conditions like cancer metastasis, in case of infections and during inflammation, and in normal and pathological bone healing.

In the field of dentistry, especially in orthodontics, the bone remodelling process is crucial for the proper alignment of teeth following various orthodontic procedures. Orthodontics is a special branch of dentistry that is focussed on the misalignment of the maxilla and mandible bones that leads to difficulty in grinding of food. A variety of surgical procedures are aimed at effecting this bone remodelling process to help in proper tooth alignment such as piezocision (corticotomy), which is a minimally invasive approach wherein incisions and decortications are made along the teeth resulting in decreased recovery time and accelerated tooth movement for improved alignment (Charavet et al., 2016, Dibart et al., 2009).

Rodents and pig models have been employed to study the pathophysiology of bone disorders because of their close similarity to the human bone physiology (Bagi et al., 2011, Cone et al., 2017, Jilka, 2013, Pogoda et al., 2005). Especially rats and mice have been used to study orthodontic tooth disorders and their influencing factors, and assess and monitor treatment responses of the bone (Kirschneck et al., 2020, Qi et al., 2019, Ren et al., 2004, Taddei et al., 2012).

In the present work, the effects of piezocision were monitored in rats by bone SPECT/CT with ^{99m}Tc-MDP before and after treatment to investigate the impact of piezocision on tracer bone uptake as a measure of bone remodelling.

2 Methods

This section is a brief summary of relevant topics of the materials and methods of three papers originally published in Endocrine-Related Cancer (Mohan et al., 2024) and Nuklearmedizin (Beindorff et al., 2022, Mohan et al., 2020). For a detailed description of the methodology, please refer to the original publications.

All animal experiments and study protocols were approved by the local committee for animal care (LaGeSo) under application numbers G0177/18, G0353/12, G0110/15, G0011/16 and G0189/13 in accordance with the German Law for the Protection of Animals. Also, all institutional and national guidelines for the care and use of animals were followed. The animals were housed at Berlin Experimental Radionuclide Imaging Center (BERIC) with the previously described husbandry conditions (Beindorff et al., 2018, Beindorff et al., 2022), and all surgical and scintigraphic procedures were performed at BERIC under isoflurane anaesthesia.

2.1 PET/CT for monitoring tumor growth and metabolism, differentiation, and receptor expression in NET before and during tumor treatment

2.1.1 Establishment of orthotopic xenograft mouse tumor model

Human pancreatic undifferentiated NET cell lines BON1 KDMSO (everolimus sensitive) and BON1 RR2 (everolimus resistant) were used. All cell culture protocols were followed as previously published (Mohan et al., 2024). Everolimus resistance in BON1 RR2 cells was maintained by continuous administration of 10 nM of everolimus throughout the cell culture. Antibiotic, antifungal and everolimus administration were discontinued 48 hours before inoculation of the cells into the pancreas in order to reduce their influence on tumor growth in the animal. Orthotopic transplantation of two million cells was performed in a total of 74 severe combined immune deficient (SCID) mice.

2.1.2 Chemotherapy regimen

Mice were divided into four different treatment regimens namely placebo, everolimus, alpelisib and combination of everolimus and alpelisib. Animals of both cell lines were dis-

tributed into each treatment group as follows: BON1 KDMSO; placebo n = 10, everolimus n = 10, alpelisib n = 8, and combination of everolimus with alpelisib (combination) n = 10; BON1 RR2; placebo n = 10, everolimus n = 8, alpelisib n = 8, and combination n = 10. Everolimus and alpelisib concentrations were calculated for a 30 g mouse in accordance with the standard dose concentrations for humans, and all drug concentrations were formulated in DMSO and corn oil and adjusted for total oral drug volume of 100 µl for minimally invasive oral gauzing (Mohan et al., 2024).

Oral weight-adapted chemotherapy was started upon attainment of a minimum tumor size of approximately 140 mm^3. Chemotherapy was performed until the tumor attained a size of 1900-2000 mm^3 or till other termination criteria were reached.

2.1.3 Tumor growth monitoring, and radionuclide imaging with PET/CT and SPECT/CT

Sequential magnetic resonance imaging (MRI) was performed for monitoring tumor growth kinetics. Tumor volume was measured by T2 weighted fast spin echo sequences (parameters see Table 2). Initial MRI was performed 18-25 days post tumor cell inoculation, and subsequently every 1-2 weeks.

Imaging time points were defined as baseline (T0), time point 1 (T1) and final time point 2 (T2) based on the time taken to reach a specific tumor volume irrespective of the cell lines. T0 was defined as the time when tumor volume reached approx. 60 mm^3, and radionuclide PET/CT imaging with ^{18}F-FDG (viability; blood glucose values were measured before tracer administration) and ^{68}Ga-DOTATOC (SSTR expression) and renal SPECT scintigraphy (kidney toxicity) with ^{99m}Tc-MAG3 were performed. Thereafter, oral chemotherapy was started in all treatment groups. The time point (T1) was defined as the time when the first animal reached a tumor size of 1600 mm^3. All animals underwent all radionuclide imaging procedures at T1 again. An individualized final time point T2 for PET/CT imaging was decided for each animal based on either the tumor volume close to 2000 mm^3 or the time point 20 weeks post tumor cell inoculation, whichever was reached first. This time point T2 was also used for the calculation of the overall survival.

Table 2: Tumor Imaging Parameters

Relevant parameters for MRI, PET and CT imaging on dedicated small animal imaging scanners.

Imaging Modality	Sequence / Radiopharmaceutical	Scan and Reconstruction Parameters
MRI	T2 weighted Fast Spin Echo (T2w, FSE)	Matrix: 256 x 256 x 48, repetition time (TR): 3000-5000 ms, averages: 4
PET	^{68}Ga-DOTATOC & ^{18}F-FDG	OSEM algorithm, 8 iterations, 6 subsets, with attenuation and random corrections
CT	CT	45 kVp, 240 projections, 500 ms exposure time, pitch 1, binning ratio of 1:4

own representation: AM. Mohan

2.1.4 Tumor immune-histology

For immuno-histological analysis, tumors (n = 69) were evaluated by hematoxylin-eosin (HE) staining, Ki-67 tumor proliferation and SSTR2 expression based on the Volante score (Mohan et al., 2024).

2.2 SPECT/CT for monitoring treatment associated kidney toxicity and bone metabolism

2.2.1 Renal scintigraphy

For establishing normal renal function values in SCID mice in both sexes, 12 female and 12 male animals underwent ^{99m}Tc-MAG3 renal SPECT scintigraphy (Mohan et al., 2020).

Based on this normal data base in SCID mice, renal treatment-related toxicity could then be evaluated for both the various treatment regimens with alpelisib (Mohan et al., 2024) and ^{177}Lu-SSA (Mohan et al., 2020).

For treatment with alpelisib and everolimus, the mice of all four treatment groups underwent ^{99m}Tc-MAG3 renal scintigraphy pre and post oral chemotherapy at time points T0 and T1 (see also 2.1.3).

For evaluation of ^{177}Lu-SSA PRRT kidney toxic effects, six female SCID mice xenografted with pancreatic NET SSTR expressing tumors (orthotopic = 4, subcutaneous = 2) underwent semi-stationary dynamic SPECT imaging with ^{99m}Tc-MAG3 1-5 months after treatment with either 30 MBq ^{177}Lu-DOTATOC (n = 5) or 20 MBq ^{177}Lu-DOTA-JR11 (n = 1).

Semi stationary SPECT imaging with ^{99m}Tc-MAG3 was carried out in a similar manner as already published (Mohan et al., 2020, Mohan et al., 2024). The mice underwent imaging either on a single bed or in a mouse hotel (3 mice per bed position at one time point) under isoflurane anaesthesia. Immediately following the start of semi stationary SPECT acquisition, 29-50 MBq of ^{99m}Tc-MAG3 was injected intravenously into the tail vein fitted with a catheter. The different parameters of SPECT acquisition for both single bed and mouse hotel are described in Table 3.

2.2.2 Skeletal scintigraphy

In order to monitor the effects of piezocision treatment on tooth movement and bone remodelling, piezocision was performed in 10 male Wistar rats. The rats underwent surgical treatment at 10 weeks of age under general anaesthesia. The exact surgical procedure of the orthodontic appliance which was placed between the incisor and the three molars tooth's on each side of the maxilla is described in detail elsewhere (Papadopoulos et al., 2021). Following insertion of the orthodontic appliance, the cortical bone was exposed and piezocision was carried out with a piezotome 2 mm mesial from the mesial root of the first molar (Papadopoulos et al., 2021).

The whole experiment was planned in a longitudinal fashion and hence each rat was followed up with SPECT/CT imaging with ^{99m}Tc-MDP at three different time points. Baseline imaging (T0) was performed before the application of orthodontic appliances and piezocision, and T1 was carried out after 2 weeks and T2 after 4 weeks post piezocision. T0 is representative of normal ^{99m}Tc-MDP uptake in the bones, which serves as control for the timepoints T1 and T2 for assessing bone remodelling after piezocision.

SPECT imaging of the head and neck region was performed followed by a CT scan with a dedicated small animal SPECT/CT scanner (NanoSPECT/CTplus, Mediso, Hungary) fitted with a nine pinhole aperture (rat high resolution, d = 1.5 mm) 45 min after injection

of approx. 140 MBq of ^{99m}Tc-MDP into the tail vein. The relevant SPECT and CT imaging parameters are listed in Table 3.

Table 3: Animal SPECT Imaging Parameters

SPECT and CT imaging protocols with different radiopharmaceuticals employed in the studies with their respective scan parameters.

Imaging Modality	Sequence / Radiopharmaceutical	Scan and Reconstruction Parameters
SPECT	^{99m}Tc-MAG3; single bed	10 × 20 s (10 s per detector position) 25 × 50 s (25 s per detector position)
SPECT	^{99m}Tc-MAG3; mouse hotel	15 × 10 s (10 s per detector position) 25 × 25 s (25 s per detector position)
SPECT CT	^{99m}Tc-MDP CT	20 min SPECT, 360 projections 55 kVp, 1500 ms exposure time

own representation: AM. Mohan

2.3 Image Analysis

Radionuclide images were quantified using PMOD 3.5 software (PMOD Technologies Ltd., Switzerland). The tumors were evaluated for size/volume (MRI), viability (^{18}F-FDG PET) and SSTR expression (^{68}Ga-DOTATOC PET) by outlining a volume of interest (VOI) around the tumor in all respective planes of the whole tumor. The tumor uptake by the different tracers is expressed as standardized uptake value (SUV) of the 10 voxels showing the highest radioactivity within the VOI (SUV_{10}) (Mohan et al., 2024).

Renal SPECT images were analysed using Matlab R2017b (The Math-Works Inc., Natick, Massachusetts, United States). The uptake of ^{99m}Tc-MAG3 in the kidneys was quantified by manual contouring of a VOI around the kidneys. Accordingly, the time activity curves (TAC) were generated for each kidney by plotting the radioactivity of each VOI against the time thereby generating the renal function parameters T_{max}, T_{50} and T_{25} representing the time of the maximum of the curve, the time of 50% decrease (50% uptake) from T_{max} and the time of 75% decrease (25% uptake) of T_{max}, respectively (Mohan et al., 2020, Mohan et al., 2024).

Quantification of ^{99m}Tc-MDP uptake in the bones was carried out in a similar way by a manually drawn VOI, and the values are expressed as injected activity per ml (%IA_{max10}/ml) based on the 10 voxels with the highest radioactivity within the VOI (Beindorff et al., 2022).

2.4 Statistics

Statistical analyses were performed with Statistical Package for Social Sciences (SPSS) software version 21.0 or 28.0 and with R 3.1.3 (The R Foundation for Statistical Computing) programming software as indicated in the respective publications (Beindorff et al., 2022, Mohan et al., 2020, Mohan et al., 2024).

Descriptive data are expressed as median, interquartile range [IQR, 25th-75th percentile], minimum and maximum (min-max). Differences between groups were analysed using non-parametric Mann-Whitney U and Kruskal Wallis tests while Wilcoxon and Analysis of Variance (ANOVA) tests were applied to test for differences within the same groups. Survival analysis and the respective survival curves were generated using Kaplan-Meier analysis. Spearman's rho correlation coefficient was employed for testing nonparametric data correlations. A statistical level of significance was set at ≤0.05 and a level of tendency at ≤0.1. For further details, see the respective publications (Beindorff et al., 2022, Mohan et al., 2020, Mohan et al., 2024).

3 Results

This section is a summary of results of three papers originally published in Endocrine-Related Cancer (Mohan et al., 2024) and Nuklearmedizin (Beindorff et al., 2022, Mohan et al., 2020) and represents the main points of the findings relevant for the understanding of the work and the discussion. For a detailed description of the results, please refer to the original publications.

3.1 PET/CT for monitoring tumor growth and metabolism, differentiation, and receptor expression in NET

3.1.1 Tumor growth kinetics

By monitoring the tumor growth kinetics by sequential MR imaging it was observed that similar to in-vitro cell culture assays, the everolimus sensitive BON1 KDMSO tumors grew faster than the everolimus resistant BON1 RR2 tumors (p = 0.087; trend) (Aristizabal Prada et al., 2018). Accordingly, the baseline timepoint T0, i.e. before initiation of oral treatment and radionuclide imaging with a minimum target tumor size of 60 mm^3, was attained earlier by BON1 KDMSO tumors at 18-28 days than by BON1 RR2 tumors at 21-34 days. Consequently, at T1 in BON1 KDMSO animals the tumor volume was 2000 mm^3 [1926-2000] 1384-2000 for placebo while BON1 RR2 animals exhibited smaller tumor sizes of 1400 mm^3 [921-2000] 457-2000 for placebo at T1.

3.1.2 Tumor Therapy and Blood Glucose Levels

PI3kα isoform inhibitors including alpelisib are known to induce hyperglycemia (Nunnery and Mayer, 2019), and everolimus resistance is mediated through the GSK-3 pathway (Aristizabal Prada et al., 2018). Both of these phenomenons could eventually influence the glucose metabolism, and hence blood glucose values were obtained.

Pooled BON1 KDMSO (123 mg/dl [109-137] 80-159) and BON1 RR2 data (117 mg/dl [100-129] 94-207, p = 0.215) revealed no significant differences at baseline. Similarly, no significant differences were found between the different treatment groups for both cell lines at T0.

When comparing the glucose values between the treatments across the cell lines, after 4 weeks of treatment BON1 RR2 alpelisib treated mice had significantly lower glucose

levels (83 mg/dl [75-90] 67-103) compared to their BON1 KDMSO counterparts (145 mg/dl [115-177] 93-254, $p < 0.001$). Furthermore, BON1 RR2 mice under everolimus treatment exhibited lower blood glucose levels at T1 (100 mg/dl [65-114] 54-116) compared to T0 (117 mg/dl [104-147] 97-152, $p = 0.04$).

3.1.3 Survival analysis

Survival analysis was carried out based on timepoint T2. Survival curves from Kaplan-Meier analysis (Fig. 1) clearly demonstrate that placebo treated BON1 KDMSO (median 42 d) animals had a significantly shorter survival than BON1 RR2 placebo treated mice (53 d, $p < 0.001$).

In BON1 KDMSO animals, when compared to placebo, significantly increased survival was observed not only with everolimus (44 d, $p = 0.002$), but also with alpelisib (53 d, $p < 0.001$) and the combination treatment (52 d, $p < 0.001$). However, no significant difference in survival was achieved between alpelisib and combination treatment ($p = 0.675$). Interestingly, both alpelisib ($p = 0.027$) and combination treatment ($p = 0.023$) prolonged survival compared to everolimus.

In BON1 RR2 animals, the combination treatment (69 d) only was shown to significantly prolong life compared to placebo (53 d, $p < 0.001$), everolimus (56 d, $p < 0.001$) and alpelisib (61 d, $p = 0.019$) while no significant difference in survival between placebo, everolimus, and alpelisib was observed. Thus, alpelisib alone had no significant survival benefit in everolimus resistant tumors. It is important to note that two BON1 RR2 animals under combination treatment survived 20 weeks post-surgery without attaining a tumor size of 2000 mm^3.

Furthermore, metastases formation was observed 58-132 d after surgery in both cell lines: One animal each with BON1 KDMSO tumors treated with everolimus, alpelisib and combination treatment, and five BON1 RR2 animals, one treated with alpelisib and three with combination treatment presented with liver metastases, one animal also developed additional peritoneal metastases.

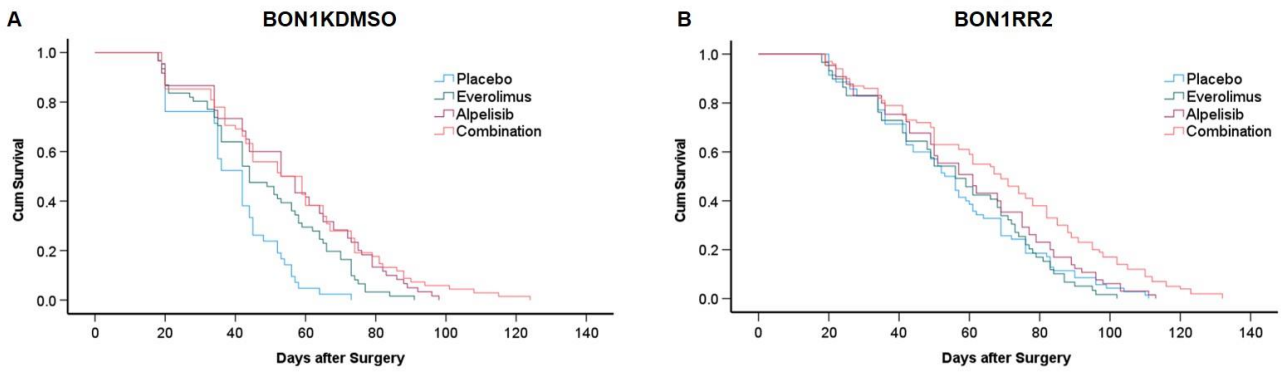

Figure 1: Survival Analysis

Kaplan-Meier survival curves depict survival for (A) BON1 KDMSO and (B) BON1 RR2 tumors for the respective treatment group. In BON1 KDMSO, survival benefit was observed for everolimus ($p = 0.002$), alpelisib ($p < 0.001$) and combination therapy ($p < 0.001$) compared to placebo, and for alpelisib ($p = 0.027$) and combination therapy ($p = 0.023$) compared to everolimus. In BON1 RR2, the combination therapy only increased survival ($p < 0.02$). (from Mohan et al. (Mohan et al., 2024))

3.1.4 Tumor SSTR expression

^{68}Ga-DOTATOC uptake as a marker for SSTR expression is listed in Table 4 for all time points for the respective cell lines and treatment groups. PET analysis across all the treatment groups showed no relevant ^{68}Ga-DOTATOC uptake, neither in BON1 KDMSO nor in BON1 RR2 animals, over the entire treatment period, thus, indicating no significant changes in SSTR tumor expression over time and during treatment.

However, one animal each from BON1 RR2 alpelisib and combination treatment revealed a high ^{68}Ga-DOTATOC SUV_{10} at T2 (28.9) and T1 (16.2), respectively. Figure 2 demonstrates the negligible ^{68}Ga-DOTATOC uptake in the tumors at all time points indicating insufficient SSTR expression on the tumor surface for DOTATOC binding.

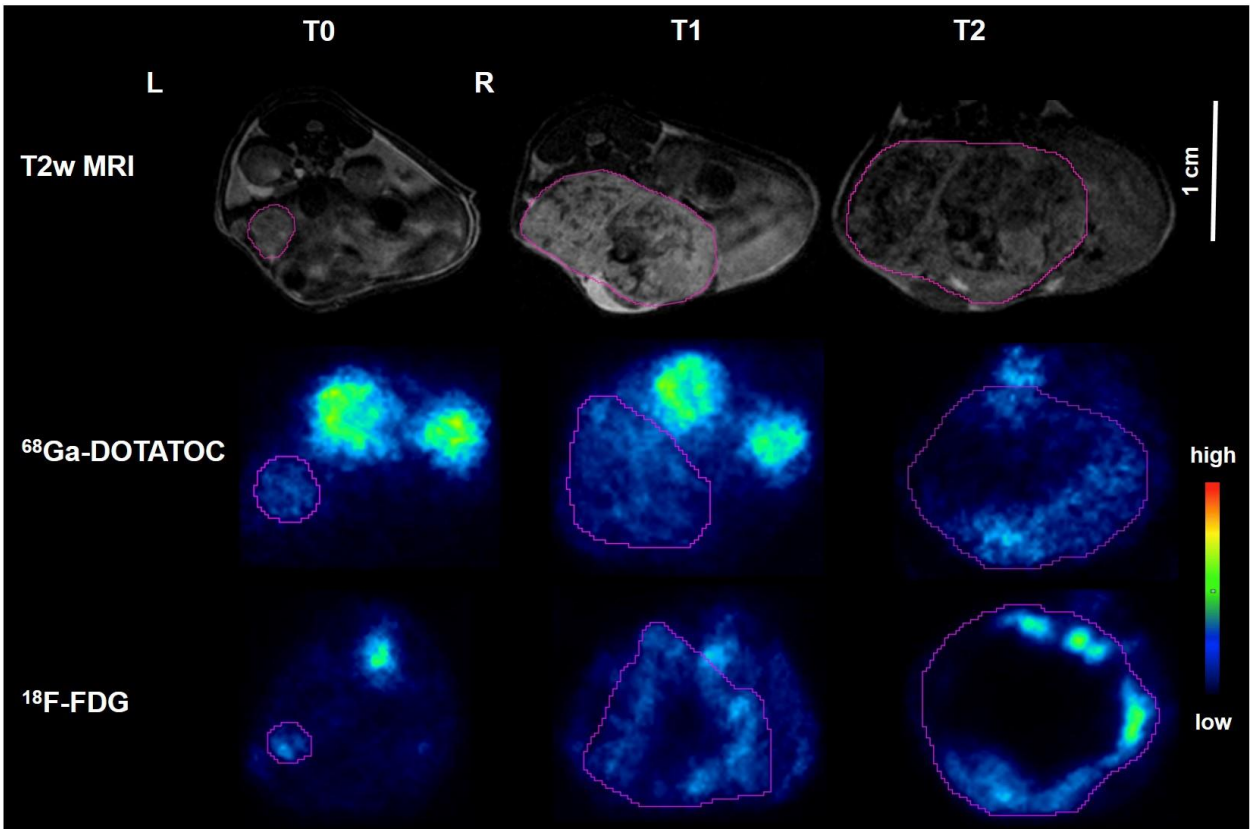

Figure 2: Tumor Differentiation

MRI, ^{68}Ga-DOTATOC and ^{18}F-FDG images of an animal that underwent combination therapy with everolimus + alpelisib at time points T0 (prior to treatment initiation), T1 (4 weeks post treatment) and T2 (before termination). The tumors are outlined in each image with a pink VOI, the respective tumor volumes were approx. 63 mm^3 at T0, 961 mm^3 at T1 and 1803 mm^3 at T2. ^{68}Ga-DOTATOC tumor uptake (SUV_{10}) was 1.3 at T0, 1.1 at T1 and 0.8 at T2. ^{18}F-FDG tumor SUV_{10} was 3.8 at T0, 4.3 at T1 and 4.2 at T2. (own figure by AM. Mohan)

Table 4: ^{68}Ga-DOTATOC Tumor Uptake

^{68}Ga-DOTATOC uptake (SUV_{10}) in the tumors indicating SSTR expression at time points T0 (baseline), T1 (4 weeks after treatment) and T2 (before euthanasia) of both everolimus sensitive (BON1 KDMSO) and everolimus resistant (BON1 RR2) tumor cell lines. Each set of data consists of median and interquartile range [25th-75th].

	BON1 KDMSO			BON1 RR2		
	T0	**T1**	**T2**	**T0**	**T1**	**T2**
Placebo	0.6 [0.4-0.8]	0.9 [0.4-1.2]	1.5	0.8 [0.6-0.9]	1.0 [0.8-1.1]	1.1 [0.8-1.1]
Everolimus	0.6 [0.4-0.9]	0.6 [0.5-0.8]	0.9 [0.5-4.9]	0.7 [0.5-0.9]	0.7 [0.7-1.3]	0.8 [0.7-1.1]
Alpelisib	0.6 [0.5-0.7]	0.8 [0.6-1.1]	0.8 [0.6-4.1]	0.7 [0.5-0.8]	0.9 [0.7-1.2]	0.9 [0.7-21.9]
Combination	1.2 [0.5-1.4]	0.8 [0.6-0.9]	0.7 [0.5-0.8]	0.9 [0.7-1.5]	1.1 [0.8-1.4]	0.8 [0.5-1.0]

(from Mohan et al. (Mohan et al., 2024))

3.1.5 Tumor Glucose metabolism and viability

Tumor viability data represented by ^{18}F-FDG uptake is shown in Table 5, and characteristic ^{18}F-FDG tumor uptake with development of necrosis over the monitoring period is depicted in Fig. 2.

Pooled data analysis at T0 revealed that everolimus sensitive BON1 KDMSO tumors had a higher uptake (3.3 [2.9-3-7] 1.4-4.1) of ^{18}F-FDG uptake than the everolimus resistant BON1 RR2 tumors (2.5 [2.2-3.4] 0.8-4.0; p = 0.025). This supplements the more aggressive nature and faster growth kinetics of the everolimus sensitive tumors as observed by MRI.

After start of treatment, no further significant differences were observed at T1 and T2 between the two cell lines. Also no differences in ^{18}F-FDG uptake were seen between the different treatment groups in BON1 KDMSO animals at all time points.

In contrast, in BON1 RR2 animals, an increase in ^{18}F-FDG uptake from T0 to T1 was observed in placebo (p = 0.003), alpelisib (p = 0.035) and combination treatment (p =

0.006) while only a potentially higher ^{18}F-FDG uptake at T1 compared to T0 was observed in everolimus treated BON1 RR2 mice (p = 0.051). In the further course of treatment, image analysis at T2 showed no significant changes.

Table 5: ^{18}F-FDG Tumor Uptake

^{18}F-FDG tumor uptake (SUV_{10}) indicating tumor viability at time points T0 (baseline), T1 (4 weeks after treatment) and T2 (before euthanasia) of both everolimus sensitive (BON1 KDMSO) and everolimus resistant (BON1 RR2) cell lines. Each set of data consists of median and interquartile range [25th-75th]. * p<0.01 and # p=0.051 between T0 and T1 within a treatment group.

	BON1 KDMSO			BON1 RR2		
	T0	**T1**	**T2**	**T0**	**T1**	**T2**
Placebo	3.1 [2.9-3.4]	5.0 [4.4-5.5]	3.4	3.5 * [2.3-3.9]	4.6 [3.7-5.4]	4.3 [3.6-4.9]
Everolimus	3.5 [2.4-3.8]	3.9 [2.8-5.6]	4.4 [3.1-5.3]	2.4 # [2.1-3.4]	4.5 [4.0-5.4]	4.3 [3.6-5.8]
Alpelisib	3.5 [3.1-3.7]	3.7 [2.7-5.3]	2.4 [1.8-3.5]	2.5 * [2.2-3.2]	4.3 [2.8-5.7)	2.8 [2.0-4.0]
Combination	3.1 [2.9-3.6]	4.4 [2.4-5.1]	2.7 [1.4-3.7]	2.4 * [1.5-3.4]	3.9 [3.3-4.9]	2.8 [2.6-4.2]

(from Mohan et al. (Mohan et al., 2024))

3.1.6 Tumor Immuno-Histology

Immunohistochemical staining revealed that most of the tumors of both cell lines exhibited morphological characteristics of a neuroendocrine carcinoma. Accordingly, most of the tumors (67/69) had a varying amount of necrosis between 30-90%, which is in line with the findings of MRI and ^{18}F-FDG PET. Furthermore, the tumors were characterized in 85±12.5% as high level (> 20%) Ki-67 expression.

No significant differences were found in Ki-67 expression between BON1 KDMSO and BON1 RR2 tumors (BON1 KDMSO 90% [85-90] 30-95, BON1 RR2 90% [85-90] 40-98,

p = 0.493). Interestingly, eight animals [BON1 KDMSO (2x everolimus, 1x combination), BON1 RR2 (2x placebo, 1x everolimus, 2x combination)] expressed characteristics of mixed endocrine/exocrine tumors instead of pure neuroendocrine carcinoma. Based on the WHO classification of digestive system tumors, these characteristics adhere to the criteria of human MiNEN (mixed neuroendocrine-non-neuroendocrine neoplasm of the pancreas) consisting of an exocrine component of 30% coupled with gland formation and cystic features (Nagtegaal et al., 2020).

Consistent with NEC morphology, almost all tumors of both cell lines across all treatment groups had a low SSTR expression of 10-30%. Volante scoring of SSTR quantification showed that only 8 tumors of all four treatment groups of BON1 RR2 cells had a Volante score 3 (> 50% of positive cells) while 54 tumors from both cell lines presented with a Volante score 2 (< 50% of positive cells) and 7 tumours with a Volante Score 0. Figure 3 shows representative immuno-histochemical tumor sections.

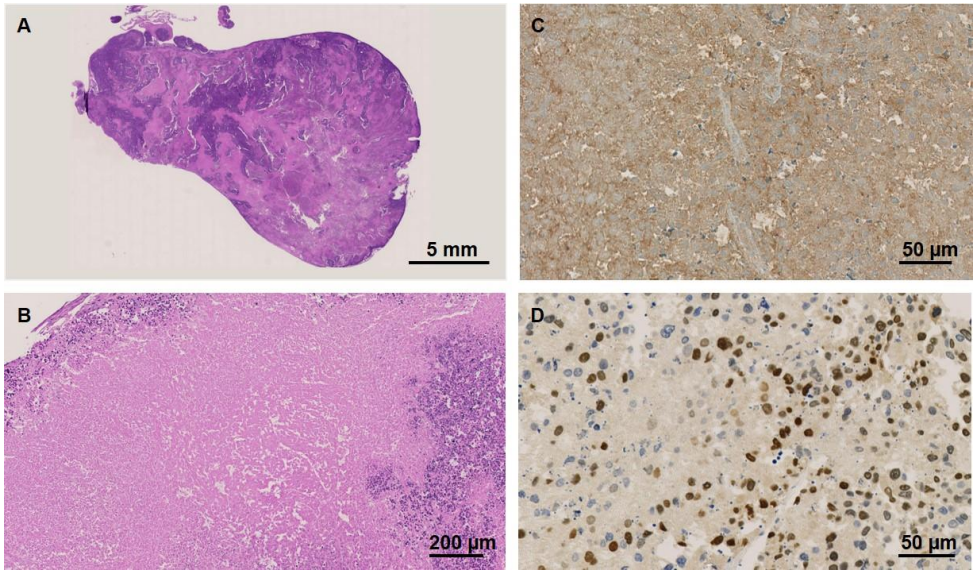

Figure 3: Tumor Histology

(A) Hematoxylin-eosin staining of a BON1 KDMSO everolimus treated tumor 81 d after surgery, showed areas of necrosis, (B-D) BON1 RR2 combination treatment (everolimus + alpelisib) 132 d after surgery: (B) hematoxylin-eosin staining, (C) SSTR2 staining with negligible SSTR2 expression, (D) highly positive Ki-67 staining. (from Mohan et al. (Mohan et al., 2024))

3.2 SPECT/CT for monitoring treatment associated kidney toxicity and post-interventional bone metabolism

3.2.1 Renal function in normal male and female SCID mice

In order to establish normal renal function values in SCID mice 12 healthy male and female SCID underwent ^{99m}Tc-MAG3 scintigraphy. Time activity curves (TAC) revealed a normal uptake characterized by a steep increase in the curves depicting optimal absorption followed by steep decrease in renal activity, which corresponds to a good clearance of the tracer from the kidneys. The left and right kidneys TAC (Fig. 4A) were congruent in nature. Interestingly, no significant differences were found between male and female SCID mice with respect to maximum tracer uptake in the kidney (T_{max}, p = 0.14) while a tendency for delayed 50% tracer clearance (T_{50} (p = 0.07)) was observed in male SCID mice. Similarly, male SCID mice (7.8 [7.3–9.2] 6.2–12.9) also exhibited a significantly delayed T_{25} clearance time compared to female mice (6.5 [5.9–7.2] 4.9–7.8, p<0.01). Table 6 summarizes renal function values of SCID mice pertaining to both sexes.

Table 6: Normal Renal Function Values

^{99m}Tc-MAG3 renal uptake of 3-month-old healthy SCID mice with respect to sex, and 5-10 month-old ^{177}Lu- somatostatin receptor ligand treated SCID mice. Each set of data includes the median, interquartile range [IQR], min-max for T_{max}, T_{50} and T_{25} in minutes; (+ p ≤ 0.05 between sexes within the strain; # p ≤ 0.05 between mice with ^{177}Lu-SRL treatment and healthy SCID mice).

Kidney uptake		SCID	SCID (^{177}Lu-SRL treatment)
females	**T_{max}**	1.4 [1.3-1.5] 1.2-5.3	2.0 [1.4-2.7] 1.3-6.9
	T_{50}	3.8 [3.5- 4.3] 3.0- 4.9	6.3 [4.5-10.1] 3.4-11.6 #
	T_{25}	6.5 [5.9-7.2] 4.9-7.8 */+	10.5 [7.7-19.3] 5.8-19.6 #
males	**T_{max}**	1.6 [1.4-1.7] 1.2-2.0	
	T_{50}	4.5 [4.0- 5.0] 2.9-6.1	
	T_{25}	7.8 [7.3-9.2] 6.2-12.9	

(from Mohan et al. (Mohan et al., 2024))

3.2.2 Assessment of renal function after PRRT treatment

Analysis of kidney parameters in mice that underwent ^{177}Lu-SSA treatment revealed an altered renal function that is depicted in the TAC in comparison to normal healthy female SCID mice (Fig. 4). Time activity curves (TAC) from ^{177}Lu-SSA treated mice also showed an incongruence between the right and left kidneys uptake and clearance (Fig. 4B). Mice that underwent PRRT had a slightly delayed T_{max} of 2.0 min ([1.4–2.7] 1.3–6.9) compared to healthy female SCID mice who reached T_{max} at 1.4 min ([1.3–1.5] 1.2–5.3, p = 0.15). Time activity curves also revealed a less steeper slope indicating a delayed clearance reaching T_{50} (p = 0.02) and T_{25} (p = 0.01) by 2.5 min and 4.1 min later, respectively, in comparison to healthy female SCID mice.

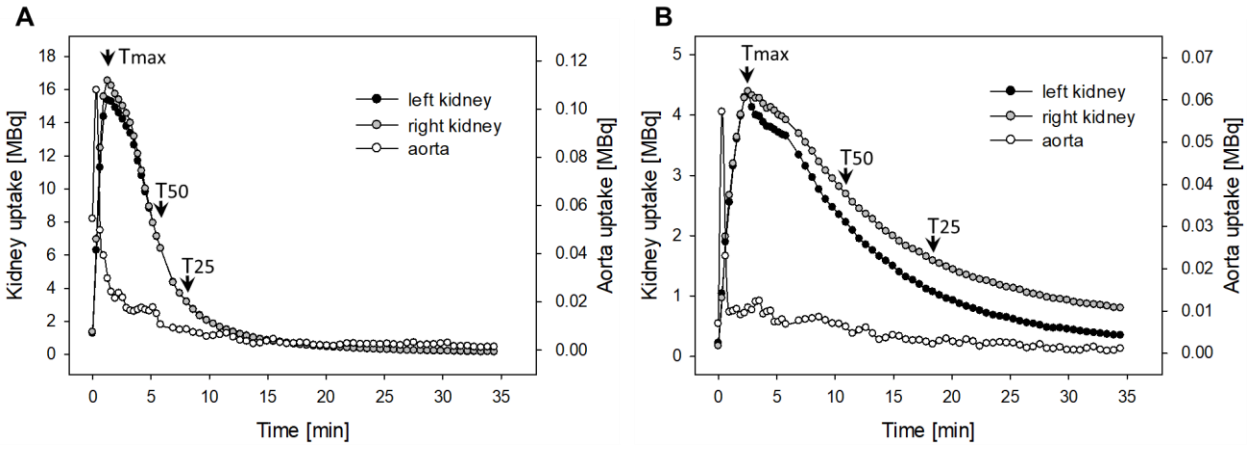

Figure 4: Renal Time Activity Curves

Time activity curves (TAC) of a normal healthy 3-month-old female SCID mouse after injection of 68 MBq ^{99m}Tc-MAG3 (A). TAC from an 11-month-old female SCID mouse after injection of 18 MBq ^{99m}Tc-MAG3 (B). ^{99m}Tc-MAG3 was performed 5 months after ^{177}Lu-DOTA-JR11 treatment (two cycles with 23 and 20 MBq three months apart) and shows delayed uptake and excretion in comparison to a normal SCID mouse. (from Mohan et al. (Mohan et al., 2020))

3.2.3 Assessment of renal function after chemotherapy

Four mice of the BON1 RR2 groups underwent renal scintigraphy prior to laparotomy in order to rule out variations from the normal SCID mouse distribution and kidney function. Additionally, in order to exclude an influence of surgery with tumor cell inoculation, these 4 mice were also compared with the baseline renal function values of 31 mice after inoculation of BON1 RR2 cells at T0 (pretreatment). Data analysis showed no significant differences for either T_{50} (p = 0.262) or T_{25} (p = 0.379) clearance between pre-surgery and

normal SCID mice. However, BON1 RR2 mice reached T_{max} significantly later by 0.4 min (1.8 [1.5-2.0] 1.5-2.1) than the normal native SCID mice (1.4 [1.3-1.5] 1.2-5.6, p = 0.02). However, no significant difference in kidney function was observed longitudinally for either T_{max} (p = 0.326), T_{50} (p = 0.599) or T_{25} (p = 0.599) between pre-surgery and T0 time point (post surgery but pretreatment), consequently, excluding a relevant impact of surgery on kidney function.

Furthermore, renal function was evaluated pre (T0) and post treatment (T1) in mice undergoing different oral therapies namely placebo, everolimus, alpelisib and combination treatment for undifferentiated NET tumors. It was observed that oral chemotherapy was well tolerated under all treatments with no impounding renal toxicity. None of the treatments had a significant effect on T_{max} in either cell line at T1 when analyzing the single groups. Only the analysis of pooled data of all animals treated with one therapy, that is all animals with BON1KDMSO and BON1RR2 tumors undergoing one treatment regimen, revealed that alpelisib significantly delayed T_{50} (6.1 min ([4.3-8.5] 3.8-25.8; p = 0.013) and T_{25} (10.1 min ([7.3-17.9] 6.2-44.2; p = 0.013) post treatment in comparison to pretreatment (T_{50} 4.1 min [3.7-5.7] 2.5-8.7; T_{25} 6.8 min [6.0-9.6] 4.2-14.8). Interestingly, this effect was no longer found when the animals were analyzed separately by the cell lines. Moreover, this effect on clearance was also not eminent with any of the other treatment regimens when using pooled data. For further details, please see Mohan et al. (Mohan et al., 2024).

3.2.4 ^{99m}Tc-MDP bone uptake for monitoring orthodontic piezocision

Analysis of pooled data exhibited a significant increase in ^{99m}Tc-MDP uptake from T0 (pre-operative; 3.2 [2.8–3.9] 2.6–4.9) to T1 (4.4 [3.8–4.6] 3.4–4.8; p = 0.001) due to bone surgery. In the further 2 weeks of healing, there was only a non-significant decrease in uptake from T1 (2 weeks) to T2 (4 weeks; 3.8 [3.1–4.4] 2.8–4.8, p = 0.116). More interesting, ^{99m}Tc-MDP bone scintigraphy revealed no significant differences in bone uptake in the maxilla after orthodontic surgery in the two groups with or without piezocision up to four weeks after surgery. Table 7 summarizes ^{99m}Tc-MDP uptake values for all time points T0, T1 and T2, and Figure 5 shows a representative SPECT/CT image depicting normal ^{99m}Tc-MDP uptake predominantly accumulating in the molar teeth at time point T0.

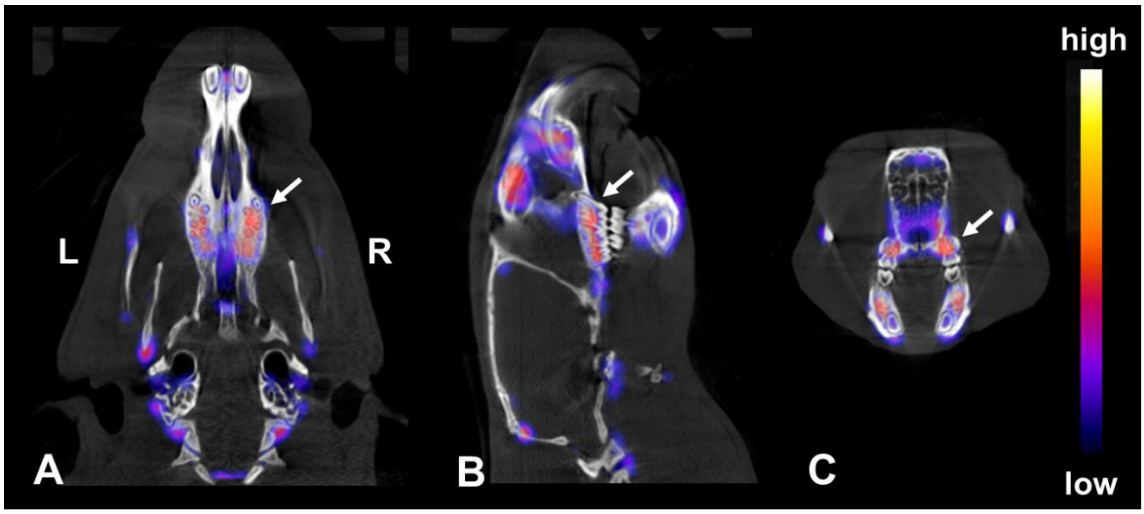

Figure 5: Skeletal Scintigraphy

SPECT/CT images of the head-and-neck region depicting ^{99m}Tc-MDP bone distribution before placement of the orthodontic appliance, in coronal (A), sagittal (B) and transverse (C) projections in a 10-month-old male rat showing normal bone uptake 48 min after intravenous injection of 186 MBq. The white arrow indicates the first molar on the right side of the upper jaw. L = left, R = right (from Beindorff et al. (Beindorff et al., 2022))

Table 7: ^{99m}Tc-MDP Bone Uptake

^{99m}Tc-MDP maxilla uptake data with and without piezocision at T0 = before, T1 = 2 weeks after, and T2 = 4 weeks after placement of the orthodontic appliances in 10 male Wistar rats. Each set of data includes the median (%IA/ml$_{max10}$), interquartile range [IQR], minimum - maximum.

	T0		T1		T2	
Piezocision	Without	With	Without	With	Without	With
Median	3.1	3.3	4.3	4.5	4.0	3.7
IQR	2.8-3.9	2.9-4.3	3.8-4.5	3.7-4.6	3.1-4.5	3.0-4.4
min-max	2.6-4.7	2.7-4.9	3.4-4.8	3.5-4.7	2.8-4.8	2.8-4.8
p-value	0.083		0.285		0.062	

(from Beindorff et al. (Beindorff et al., 2022))

4 Discussion

4.1.1 Translational Molecular Imaging

Molecular imaging is the non-invasive visual and quantitative characterization of a specific biological process happening at a cellular or molecular level. In the field of precision medicine, disease-specific biomarkers for a given pathological condition are crucial for the proper management of patients as biomarkers have been found to affect prognosis, survival and quality of life. The field of molecular imaging has rapidly evolved in identifying new biomarkers in vivo. Over the years, based on technological advances with respect to identification of new targets and radiochemistry, the field of molecular imaging has contributed to all branches of medicine covering neurology, nephrology, cardiology, inflammatory diseases and oncology. Thus, over time nuclear medicine and functional imaging have increased its applications from the diagnosis of hyperthyroidism and differentiated thyroid cancer with radioactive iodine (^{131}I) as starting point in the 1940s to the modern day theranostics, i.e. combined diagnostic and therapeutic approaches with radiolabelled pharmaceuticals, e.g. radiolabelled SSTR ligands in neuroendocrine tumors. This increase in the utility of molecular imaging was very much advanced with the advent of hybrid SPECT/CT and PET/CT technologies.

The overarching goal of this thesis was to translate clinically well-established PET and SPECT imaging methodologies into experimental settings for improved non-invasive, longitudinal monitoring of treatment-induced changes by using dedicated hybrid small animal PET/CT and SPECT/CT scanners.

4.1.2 Dual tracer PET imaging and SSTR (re-)expression in neuroendocrine tumors

PET imaging with ^{68}Ga-DOTATOC plays a significant role in the diagnosis, staging and follow up of well-differentiated NET due to SSTR expression and the binding affinity of ^{68}Ga-DOTATOC to SST receptors (Mohan et al., 2021) while ^{18}F-FDG has a major impact on the diagnostic workflow of poorly differentiated NET owing to their nil/negligible SSTR expression but increased metabolic glucose turnover in comparison to well-differentiated NET. An increased metabolic turnover has also been shown in neuroendocrine carcinomas (NEC) leading to high glucose intake, and, thus, high ^{18}F-FDG uptake (Kayani et al., 2008). The so-called NETPET scoring system devised by Chan et al. is highly promising

as a prognostic factor, and also serves as a predictor of overall survival (Bailey et al., 2019, Chan et al., 2017a).

One of the aims of this study was centered on the hypothesis that everolimus resistance could be circumvented by adjuvant administration of a PI3k inhibitor subsequently leading to (re-)expression of SST receptors as well (Passacantilli et al., 2014, Vandamme et al., 2016).

In our study, however, no significant re-expression of SSTR was observed by ^{68}Ga-DOTATOC PET at the cell surface receptor level after treatment with the PI3k inhibitor alpelisib in most of the animals. Moreover, constantly positive ^{18}F-FDG PET imaging also indicated negligible re-differentiation over the course of treatment. This is contrary to the in vitro findings by Nölting et al., wherein a high SSTR2 transcription was found after combined treatment with everolimus and alpelisib in native BON1 NET cells (Nolting et al., 2017). Similarly, Prada et al. also reported an increased SSTR2 transcription in everolimus resistant BON1 RR1/RR2 cell lines under combination treatment (Aristizabal Prada et al., 2018). These paradoxical findings may be addressed by the fact that an increased SSTR transcription was observed in vitro at a molecular, i.e. RNA level, which however may not be indicative for sufficient SSTR expression at the cell surface necessary for imaging with radiolabelled somatostatin analogues. This explanation is in line with our histochemical analysis which revealed that 89% of the tumors had a NEC morphology with increased Ki-67 (as reflected by high ^{18}F-FDG uptake) and necrosis (see Fig. 3) but no SSTR expression (no relevant ^{68}Ga-DOTATOC uptake). Only 11% of tumors exhibited a mixed morphology with parts of both NEC and well-differentiated NET accompanied by increased SSTR2 expression, which nicely corresponds to a positive ^{68}Ga-DOTATOC PET in 9% of the animals. Because the everolimus sensitive (BON1 KDMSO) and resistant (BON1 RR2) cell lines have been developed from the parent BON1 cell line, which is derived from a poorly differentiated NET, the positive and constantly high ^{18}F-FDG tumor uptake over the entire treatment period perfectly fits to its molecular characteristics (Aristizabal Prada et al., 2018). Thus, the histopathological results ultimately validate the sensitivity and specificity of the PET tracers ^{18}F-FDG and ^{68}Ga-DOTATOC in this experimental setting while these tracers likewise serve as reliable biomarkers for the in vivo characterization of specific tumor features.

4.1.3 Validation of cell line characteristics by imaging

Poorly differentiated NET are morphologically aggressive in nature with rapid tumor growth characteristics. Prada et al. observed an accelerated tumor growth in BON1 KDMSO cells in comparison to the everolimus resistant BON1 RR1/BON1 RR2 cells in in vitro culture experiments (Aristizabal Prada et al., 2018). This was replicated by our in vivo studies wherein tumor growth kinetics monitored with MR imaging showed that placebo-treated BON1 KDMSO tumors grew faster than placebo-treated BON1 RR2 tumors. This was also reflected in the survival curves generated by Kaplan-Meier analysis wherein BON1 KDMSO animals treated with placebo had a shorter survival than BON1 RR2 placebo animals (Fig. 1). Furthermore, everolimus treatment of BON1 RR2 tumors had no significant impact on survival in comparison to BON1 RR2 placebo as this cell line is everolimus resistant. On the other hand, a significant survival benefit of everolimus was observed in wild type BON1 KDMSO tumors (Fig. 1). Thus, our study could clearly authenticate and validate the translation of everolimus resistance from in vitro to a first ever robust everolimus resistant in vivo orthotopic tumor mouse model which can be easily characterized by imaging methods.

Further analysis of survival data revealed a significantly prolonged survival with both standalone alpelisib and combination treatment compared to placebo and to everolimus in BON1 KDMSO tumors. Interestingly, the efficacy of standalone alpelisib may eventually be translated into the clinics and used in patients as drug alternative to everolimus. In the everolimus resistant BON1 RR2 groups however only the combination treatment had a significant effect on survival. This clearly proves our hypothesis that the concomitant therapy with alpelisib and everolimus results in overcoming everolimus resistance in everolimus resistant tumors by combined blockage of PI3Kα and mTORC1 pathways, and MR imaging helped generating longitudinal tumor volume data without killing the animals at each relevant time point.

Of special note, tumor size measured by a caliper on the living mouse would not have been a reliable measure because tumor treatment effects are rather shown by the amount of tumor necrosis than simple size and volume as nicely depicted in Fig. 2. MR imaging is commonly used for quantitative morphological tumor characterization by measuring tumor volume and extent of necrosis (Ayala-Domínguez et al., 2020, Benzakoun et al., 2020). Necrosis in the centre of the tumor mass due to intratumoral hypoxia dictated by the rapidly growing tumor is a well-known feature (Yoshida et al., 2019). In our study, MR

imaging revealed distinct growth patterns presenting with a varied amount of tumor necrosis during various treatments. These results were further supplemented by PET imaging with ^{18}F-FDG which is actively taken up by living tumor cells only owing to their glucose metabolism. Hence, the necrotic part is devoid of ^{18}F-FDG uptake. Thus, MRI and ^{18}F-FDG PET imaging served as in vivo biomarkers for differentiating viable from necrotic tumor tissue helping to adequately define treatment response.

4.1.4 Renal function and toxicity

Studies have illustrated renal failure as one of the common causes of termination of chemotherapy (Sassier et al., 2015) but renal toxicity is also a well-known side effect of PRRT due to accumulation of radiolabelled peptides in the proximal convoluted tubule of the kidneys mediated by the megalin-cubilin system (Vegt et al., 2010, Vegt et al., 2011, Bergsma et al., 2016). Hence monitoring of renal function is important to attain both maximum therapeutic efficacy and minimum renal toxicity. Assessment of renal function by ^{99m}Tc-MAG3 imaging following PRRT treatment has been previously reported and is commonly applied in the management of NET patients undergoing PRRT (Werner et al., 2016). Although ^{99m}Tc-MAG3 imaging is part of the clinical workup, its application on the preclinical front was hampered so far due to the lack of normal renal function values in immuno-deficient mice. In rats and mice, sex dependent differences have been documented with respect to glomerular filtration rates, renal plasma flow and the washout of different compounds from the kidney tubules (Hackbarth et al., 1981, Hackbarth and Hackbarth, 1981, Hackbarth and Hackbarth, 1982). Sex and age related differences were also found in C57BL/6N mice for renal SPECT scintigraphy with ^{99m}Tc-MAG3 (Huang et al., 2018).

For pooled SCID mouse data in general, no significantly different normal kidney values were found in the present work in comparison to the normal data reported by Huang et al. for C57BL/6N mice (Huang et al., 2018). However, when comparing sex-related data, both significant differences between these two strains could be detected as well as significant differences between male and female SCID mice with a delayed T_{25} clearance time in male SCID mice ($p<0.01$; see Tab. 6). Thus, the initial establishment of a normal data base for renal function analysis for each different mouse strain, and for both sexes, is a prerequisite for experimental studies on kidney toxicity.

These normal values served as baseline for follow-up of renal damage in SCID mice undergoing various chemo/radiotherapy treatments. Kidneys are one of the critical organs in PRRT treatment in patients. Consequently, the ^{99m}Tc-MAG3 clearance in renal scintigraphy may be affected post PRRT (Rudisile et al., 2019). Such an effect was also observed in our study wherein SCID mice with G3 NET tumors undergoing PRRT exhibited a delayed ^{99m}Tc-MAG3 clearance (T_{50} and T_{25}) in comparison to healthy untreated SCID mice (Fig. 4, Tab. 6).

Although post treatment renal scintigraphy revealed no significant changes for T_{max} in our study on everolimus resistance in most treatment groups, alpelisib caused a significantly delayed tracer excretion with respect to T_{50} and T_{25} after 4 weeks of treatment. This is in line with frequently observed increased serum creatinine levels in clinical studies on alpelisib in breast cancer patients (Food and Drug Administration, Markham, 2019).

Thus, after establishing a normal data base for the respective experimental setting, renal ^{99m}Tc-MAG3 SPECT imaging in mice proved sufficiently sensitive for monitoring therapy-induced renal function impairment.

4.1.5 Bone Remodelling

Skeletal scintigraphy is the gold standard for visualization of bone metabolism, and a sensitive quantitative technique for detecting metabolic changes. ^{99m}Tc-MDP uptake is directly correlated to the osteoblastic turnover which is upregulated by various factors governing tooth movement (Li et al., 2018), e.g. at the areas of tension and pressure due to varying forces of orthodontic appliances (Garcia et al., 1974). Furthermore, ^{99m}Tc-MDP uptake is dependent on the stages of the bone remodelling process (Upadhyay et al., 2017). In rats, the bone formation phase during bone remodelling takes place at around 14-28 days after a respective stimulus and is characterized by increased osteoblastic activity (Ohira et al., 2020). Ohira et al. also reported that the normal time for bone mineralization ranges from 28-70 days, wherein a decrease in osteoblastic activity is observed during this period (Ohira et al., 2020). This is in accordance to our study and explains the significantly increased ^{99m}Tc-MDP uptake at 2 weeks post orthodontic procedures, which decreased at 4 weeks post treatment. However, contrary to the hypothesis that the ^{99m}Tc-MDP uptake increases with the intensity of the trauma, there was no significant effect of additional piezocision on ^{99m}Tc-MDP uptake in comparison to the side undergoing only orthodontic appliance placement. Piezocision is a procedure performed

to accelerate orthodontic tooth movement which is highly influenced by osteoclastogenesis (Papadopoulos et al., 2021). However, osteoclastogenesis primarily governs the turnover of osteoclasts at the site of bone formation and not so much osteoblasts per se, which could explain the insignificant impact of piezocision of ^{99m}Tc-MDP bone uptake. Moreover, the distinct and significant effects of the orthodontic appliances themselves may conceal the effects of additional piezocision.

Thus, bone scintigraphy was highly sensitive in detecting bone remodelling changes after surgery demonstrating an increased uptake at 2 weeks that gradually faded at 4 weeks after orthodontic appliance application with/without piezocision. However, no additional effect of piezocision on bone metabolism was observed that could be detected by bone SPECT/CT scintigraphy.

4.2. Limitations

A major and general limitation of animal studies as presented here is the usually small number of cases. Due to the very time-consuming multimodal imaging procedures, only a limited number of animals could be examined at the same time points. Although this limited the statistical significance of the results, the multimodal approach with various imaging methods and biomarkers on the other hand helped to confirm the data, so that valid statements could be made despite the small number of cases. Of interest, the major advantage of imaging with respect to the 3R concepts is that all the animals used in the different experiments were followed up longitudinally with the respective imaging methodology both at baseline and after treatment. In such longitudinal study protocols each animal served as its own control thereby helping to minimise the number of animals required per time point to obtain the required information with sufficient statistical power as achieved by dependent data.

A specific limitation of the renal SPECT imaging model is the non-feasibility of calculating the ^{99m}Tc-MAG3 clearance in analogy to patients. Clinically, the split renal function and the clearance of ^{99m}Tc-MAG3, measured in millilitre per minute, is calculated based both on the input function in the abdominal aorta and by combined blood sampling. This technique however could not be translated into mice owing primarily to the small blood volume of mice not allowing to take sufficient blood samples, secondly, the limited time resolution of SPECT imaging which does not allow to reliably measure the time-activity curve in sufficiently short time intervals of seconds and, thirdly, the limited spatial resolution of the

SPECT system causing partial volume effects due to the small diameter of the aorta. These drawbacks do not allow to precisely calculate the clearance of ^{99m}Tc-MAG3 in mice limiting the reliable and reproducible renal functional parameters to T_{max}, T_{50} and T_{25}. For a detailed discussion of this topic, please refer to Huang et al. (Huang et al., 2018).

4.3. Implications for future research

A first ever-robust everolimus resistant tumor xenograft SCID mouse model was successfully established along with preclinical imaging, and the therapeutic potential and efficacy of the PI3Kα inhibitor alpelisib in overcoming everolimus resistance was validated in vivo by this model. This has three major implications: Firstly, this model and its respective imaging procedures can be used for further preclinical mouse research on everolimus resistance. Secondly, alpelisib, so far FDA-approved for breast cancer therapy, in combination with everolimus resulted in a significantly prolonged survival of animals with everolimus resistant tumors. This clearly proves our hypothesis that the concomitant therapy with alpelisib and everolimus may overcome everolimus resistance by blockage of both PI3Kα and mTORC1 pathways, which will serve as a solid basis for further preclinical research and future clinical trials on this topic. Thirdly, alpelisib alone seems promising as a novel therapeutic approach in NET/NEC because alpelisib treated animals survived significantly longer in comparison to everolimus treated animals with everolimus sensitive tumors indicating a high anti-tumor potential of alpelisib per se. As both everolimus and alpelisib are already approved drugs, a clinical study may be the next step for investigating alpelisib versus everolimus in NET and NEC to gain data on toxicity and survival in a clinical setting.

With respect to kidney functional SPECT imaging, SCID mouse normal data for both female and male animals have been compiled for the first time using a recently established imaging protocol (Huang et al., 2018). This data will serve as a basis for monitoring kidney function during therapy in future oncological preclinical research in which immuno-compromised SCID mice with xenotransplanted human tumors play an essential role.

With respect to the overall goal of translating and implementing dedicated radionuclide imaging procedures with SPECT and PET in preclinical animal research, imaging protocols have been established and validated which can be used as a basis, and might be an inspiration for including longitudinal imaging into future experimental animal-based research for improved in vivo tumor and disease monitoring and characterization.

5 Conclusions

The overarching goal of this thesis was to translate clinically well-established PET and SPECT imaging methodologies into various experimental preclinical settings for non-invasive in vivo tumor characterization and treatment monitoring as well as detection of potential treatment-induced functional changes.

A first ever robust everolimus resistant tumor SCID mouse xenograft model was successfully established and the therapeutic potential and efficacy of the PI3Kα inhibitor alpelisib in overcoming everolimus resistance in neuroendocrine tumors was confirmed in vivo indicating that this model and its respective PET and MR imaging procedures can be used for further preclinical mouse research on this prominent topic.

With respect to kidney functional SPECT imaging with ^{99m}Tc-MAG3, SCID mouse normal data for both female and male animals have been compiled for the first time. This data served as a basis for monitoring kidney function during PRRT and chemotherapy with alpelisib in neuroendocrine tumors demonstrating that renal ^{99m}Tc-MAG3 SPECT imaging in SCID mice with xenotransplanted human tumors proved sufficiently sensitive for monitoring therapy-induced renal functional impairment.

In a third experimental setting on orthodontic piezocision, bone scintigraphy with ^{99m}Tc-MDP was highly sensitive in monitoring and detecting bone remodelling changes in rats after orthodontic surgery although no additional effect of piezocision on bone metabolism was observed that could be detected by bone SPECT imaging.

In summary, the present work clearly substantiates the preclinical use of non-invasive nuclear medicine SPECT and PET imaging procedures with dedicated small animal scanners, which allow a comprehensive analysis of reliable in vivo treatment response monitoring and detection of potential morbidities and functional changes arising from the tumor and the tumor treatment. Imaging protocols have been established and validated which can be used as a basis for including longitudinal radionuclide imaging into future experimental animal-based research.

Reference list

1. AKIROV, A., LAROUCHE, V., ALSHEHRI, S., ASA, S. L. & EZZAT, S. 2019. Treatment Options for Pancreatic Neuroendocrine Tumors. *Cancers (Basel),* 11.

2. ALSADIK, S., GNANASEGARAN, G., CHEN, L., MANDAIR, D., TOUMPANAKIS, C., CAPLIN, M. & NAVALKISSOOR, S. 2022. Safety of Peptide Receptor Radionuclide Therapy with (177)Lu-DOTATATE in Neuroendocrine Tumor Patients with Chronic Kidney Disease. *J Nucl Med,* 63**,** 1503-1508.

3. ARISTIZABAL PRADA, E. T., SPOTTL, G., MAURER, J., LAUSEKER, M., KOZIOLEK, E. J., SCHRADER, J., GROSSMAN, A., PACAK, K., BEUSCHLEIN, F., AUERNHAMMER, C. J. & NÖLTING, S. 2018. The role of GSK3 and its reversal with GSK3 antagonism in everolimus resistance. *Endocr Relat Cancer,* 25**,** 893-908.

4. AYALA-DOMÍNGUEZ, L., PÉREZ-CÁRDENAS, E., AVILÉS-SALAS, A., MEDINA, L. A., LIZANO, M. & BRANDAN, M.-E. 2020. Quantitative imaging parameters of contrast-enhanced micro-computed tomography correlate with angiogenesis and necrosis in a subcutaneous c6 glioma model. *Cancers,* 12**,** 3417.

5. BAGI, C. M., BERRYMAN, E. & MOALLI, M. R. 2011. Comparative bone anatomy of commonly used laboratory animals: implications for drug discovery. *Comp Med,* 61**,** 76-85.

6. BAILEY, D., CHAN, D., ROACH, P., SCHEMBRI, G., BERNARD, E., HSIAO, E., HAYES, A., KHASRAW, M., SAMRA, J. & PAVLAKIS, N. 2019. The Prognostic Impact of Dual FDG/Somatostatin Receptor PET in Metastatic Neuroendocrine Tumours: Updated Overall Survival from the NETPET Study. *Journal of Nuclear Medicine,* 60**,** 505-505.

7. BEINDORFF, N., BARTELHEIMER, A., HUANG, K., LUKAS, M., LANGE, C., HUANG, E. L., ASCHENBACH, J. R., EARY, J. F., STEFFEN, I. G. & BRENNER, W. 2018. Normal Values of Thyroid Uptake of 99mTechnetium Pertechnetate

SPECT in Mice with Respect to Age, Sex, and Circadian Rhythm. *Nuklearmedizin,* 57**,** 181-189.

8. BEINDORFF, N., PAPADOPOULOS, N., HOFFMANN, S., MOHAN, A. M., LUKAS, M., BRENNER, W., JOST-BRINKMANN, P. G. & PRAGER, T. 2022. Monitoring orthodontic tooth movement in rats after piezocision by bone scintigraphy. *Nuklearmedizin,* 61**,** 402-409.

9. BENZAKOUN, J., ROBERT, C., LEGRAND, L., PALLUD, J., MEDER, J. F., OPPENHEIM, C., DHERMAIN, F. & EDJLALI, M. 2020. Anatomical and functional MR imaging to define tumoral boundaries and characterize lesions in neuro-oncology. *Cancer Radiother,* 24**,** 453-462.

10. BERGSMA, H., KONIJNENBERG, M. W., VAN DER ZWAN, W. A., KAM, B. L., TEUNISSEN, J. J., KOOIJ, P. P., MAUFF, K. A., KRENNING, E. P. & KWEKKEBOOM, D. J. 2016. Nephrotoxicity after PRRT with (177)Lu-DOTA-octreotate. *Eur J Nucl Med Mol Imaging,* 43**,** 1802-11.

11. CHAN, D. L., PAVLAKIS, N., SCHEMBRI, G. P., BERNARD, E. J., HSIAO, E., HAYES, A., BARNES, T., DIAKOS, C., KHASRAW, M., SAMRA, J., ESLICK, E., ROACH, P. J., ENGEL, A., CLARKE, S. J. & BAILEY, D. L. 2017a. Dual Somatostatin Receptor/FDG PET/CT Imaging in Metastatic Neuroendocrine Tumours: Proposal for a Novel Grading Scheme with Prognostic Significance. *Theranostics,* 7**,** 1149-1158.

12. CHAN, D. L., SEGELOV, E. & SINGH, S. J. T. A. I. G. 2017b. Everolimus in the management of metastatic neuroendocrine tumours. 10**,** 132-141.

13. CHARAVET, C., LECLOUX, G., BRUWIER, A., ROMPEN, E., MAES, N., LIMME, M. & LAMBERT, F. 2016. Localized Piezoelectric Alveolar Decortication for Orthodontic Treatment in Adults: A Randomized Controlled Trial. *J Dent Res,* 95**,** 1003-9.

14. CHEN, S. H., CHANG, Y. C., HWANG, T. L., CHEN, J. S., CHOU, W. C., HSIEH, C. H., YEH, T. S., HSU, J. T., YEH, C. N., TSENG, J. H., CHEN, T. C. & YEN, T. C. 2018. 68Ga-DOTATOC and 18F-FDG PET/CT for identifying the primary

lesions of suspected and metastatic neuroendocrine tumors: A prospective study in Taiwan. *J Formos Med Assoc,* 117**,** 480-487.

15. CIOŁCZYK-WIERZBICKA, D., GIL, D., ZARZYCKA, M. & LAIDLER, P. J. H. C. 2020. mTOR inhibitor everolimus reduces invasiveness of melanoma cells. 33**,** 88-97.

16. CONE, S. G., WARREN, P. B. & FISHER, M. B. 2017. Rise of the Pigs: Utilization of the Porcine Model to Study Musculoskeletal Biomechanics and Tissue Engineering During Skeletal Growth. *Tissue Eng Part C Methods,* 23**,** 763-780.

17. CURIGLIANO, G., MARTIN, M., JHAVERI, K., BECK, J. T., TORTORA, G., FAZIO, N., MAUR, M., HUBNER, R. A., LAHNER, H., DONNET, V., AJIPA, O., LI, Z., BLUMENSTEIN, L. & ANDRE, F. 2021. Alpelisib in combination with everolimus +/- exemestane in solid tumours: Phase Ib randomised, open-label, multicentre study. *Eur J Cancer,* 151**,** 49-62.

18. DEL RIVERO, J., PEREZ, K., KENNEDY, E. B., MITTRA, E. S., VIJAYVERGIA, N., ARSHAD, J., BASU, S., CHAUHAN, A., DASARI, A. N., BELLIZZI, A. M., GANGI, A., GRADY, E., HOWE, J. R., IVANIDZE, J., LEWIS, M., MAILMAN, J., RAJ, N., SOARES, H. P., SOULEN, M. C., WHITE, S. B., CHAN, J. A., KUNZ, P. L., SINGH, S., HALFDANARSON, T. R., STROSBERG, J. R. & BERGSLAND, E. K. 2023. Systemic Therapy for Tumor Control in Metastatic Well-Differentiated Gastroenteropancreatic Neuroendocrine Tumors: ASCO Guideline. *J Clin Oncol,* 41**,** 5049-5067.

19. DIBART, S., SEBAOUN, J. D. & SURMENIAN, J. 2009. Piezocision: a minimally invasive, periodontally accelerated orthodontic tooth movement procedure. *Compend Contin Educ Dent,* 30**,** 342-4, 346, 348-50.

20. ELKABETS, M., VORA, S., JURIC, D., MORSE, N., MINO-KENUDSON, M., MURANEN, T., TAO, J., CAMPOS, A. B., RODON, J., IBRAHIM, Y. H., SERRA, V., RODRIK-OUTMEZGUINE, V., HAZRA, S., SINGH, S., KIM, P., QUADT, C., LIU, M., HUANG, A., ROSEN, N., ENGELMAN, J. A., SCALTRITI, M. & BASELGA,

J. 2013. mTORC1 inhibition is required for sensitivity to PI3K p110alpha inhibitors in PIK3CA-mutant breast cancer. *Sci Transl Med,* 5**,** 196ra99.

21. ESHIMA, D. & TAYLOR, A., JR. 1992. Technetium-99m (99mTc) mercaptoacetyltriglycine: update on the new 99mTc renal tubular function agent. *Semin Nucl Med,* 22**,** 61-73.

22. FOOD AND DRUG ADMINISTRATION, U. *HIGHLIGHTS OF PRESCRIBING INFORMATION* [Online]. Available: https://www.accessdata.fda.gov/drugsatfda_docs/label/2019/212526s000lbl.pdf [Accessed].

23. FRITSCH, C., HUANG, A., CHATENAY-RIVAUDAY, C., SCHNELL, C., REDDY, A., LIU, M., KAUFFMANN, A., GUTHY, D., ERDMANN, D., DE POVER, A., FURET, P., GAO, H., FERRETTI, S., WANG, Y., TRAPPE, J., BRACHMANN, S. M., MAIRA, S. M., WILSON, C., BOEHM, M., GARCIA-ECHEVERRIA, C., CHENE, P., WIESMANN, M., COZENS, R., LEHAR, J., SCHLEGEL, R., CARAVATTI, G., HOFMANN, F. & SELLERS, W. R. 2014. Characterization of the novel and specific PI3Kalpha inhibitor NVP-BYL719 and development of the patient stratification strategy for clinical trials. *Mol Cancer Ther,* 13**,** 1117-29.

24. GARCIA, D. A., HIGGINBOTHAM, D. J., HOUSE, J. E. & KAPUR, K. K. 1974. Tc-99m-polyphosphate bone imaging of orthodontically treated dog teeth. *American Journal of Orthodontics,* 66**,** 665-674.

25. HACKBARTH, H., BAUNACK, E. & WINN, M. 1981. Strain differences in kidney function of inbred rats: 1. Glomerular filtration rate and renal plasma flow. *Lab Anim,* 15**,** 125-8.

26. HACKBARTH, H. & HACKBARTH, D. 1981. Genetic analysis of renal function in mice. 1. Glomerular filtration rate and its correlation with body and kidney weight. *Lab Anim,* 15**,** 267-72.

27. HACKBARTH, H. & HACKBARTH, D. 1982. Genetic analysis of renal function in mice. 2. Strain differences in clearances of sodium, potassium, osmolar and free water, and their correlations with body and kidney weight. *Lab Anim,* 16**,** 27-32.

28. HINDIE, E. 2017. The NETPET Score: Combining FDG and Somatostatin Receptor Imaging for Optimal Management of Patients with Metastatic Well-Differentiated Neuroendocrine Tumors. *Theranostics,* 7**,** 1159-1163.

29. HOPE, T. A., ALLEN-AUERBACH, M., BODEI, L., CALAIS, J., DAHLBOM, M., DUNNWALD, L. K., GRAHAM, M. M., JACENE, H. A., HEATH, C. L. & MITTRA, E. S. 2023. SNMMI procedure standard/EANM practice guideline for SSTR PET: imaging neuroendocrine tumors. *Journal of Nuclear Medicine,* 64**,** 204-210.

30. HOPE, T. A., PAVEL, M. & BERGSLAND, E. K. 2022. Neuroendocrine Tumors and Peptide Receptor Radionuclide Therapy: When Is the Right Time? *J Clin Oncol,* 40**,** 2818-2829.

31. HUANG, K., LUKAS, M., STEFFEN, I. G., LANGE, C., HUANG, E. L., DORAU, V., BRENNER, W. & BEINDORFF, N. 2018. Normal Values of Renal Function measured with 99mTechnetium Mercaptoacetyltriglycine SPECT in Mice with Respect to Age, Sex and Circadian Rhythm. *Nuklearmedizin,* 57**,** 224-233.

32. JILKA, R. L. 2013. The relevance of mouse models for investigating age-related bone loss in humans. *J Gerontol A Biol Sci Med Sci,* 68**,** 1209-17.

33. KAM, B. L., TEUNISSEN, J. J., KRENNING, E. P., DE HERDER, W. W., KHAN, S., VAN VLIET, E. I. & KWEKKEBOOM, D. J. 2012. Lutetium-labelled peptides for therapy of neuroendocrine tumours. *Eur J Nucl Med Mol Imaging,* 39 Suppl 1**,** S103-12.

34. KAYANI, I., BOMANJI, J. B., GROVES, A., CONWAY, G., GACINOVIC, S., WIN, T., DICKSON, J., CAPLIN, M. & ELL, P. J. 2008. Functional imaging of neuroendocrine tumors with combined PET/CT using 68Ga-DOTATATE (DOTA-DPhe1,Tyr3-octreotate) and 18F-FDG. *Cancer,* 112**,** 2447-55.

35. KELGIORGI, D. & DERVENIS, C. 2017. Pancreatic neuroendocrine tumors: the basics, the gray zone, and the target. *F1000Res,* 6**,** 663.

36. KIRSCHNECK, C., BAUER, M., GUBERNATOR, J., PROFF, P. & SCHRODER, A. 2020. Comparative assessment of mouse models for experimental orthodontic tooth movement. *Sci Rep,* 10**,** 12154.

37. KUMAR, R., SHARMA, P., GARG, P., KARUNANITHI, S., NASWA, N., SHARMA, R., THULKAR, S., LATA, S. & MALHOTRA, A. 2011. Role of (68)Ga-DOTATOC PET-CT in the diagnosis and staging of pancreatic neuroendocrine tumours. *Eur Radiol,* 21**,** 2408-16.

38. KWEKKEBOOM, D. J., BAKKER, W. H., KOOIJ, P. P., KONIJNENBERG, M. W., SRINIVASAN, A., ERION, J. L., SCHMIDT, M. A., BUGAJ, J. L., DE JONG, M. & KRENNING, E. P. 2001. [177Lu-DOTAOTyr3]octreotate: comparison with [111In-DTPAo]octreotide in patients. *Eur J Nucl Med,* 28**,** 1319-25.

39. LEE, L., ITO, T. & JENSEN, R. T. 2018. Everolimus in the treatment of neuroendocrine tumors: efficacy, side-effects, resistance, and factors affecting its place in the treatment sequence. *Expert Opin Pharmacother,* 19**,** 909-928.

40. LI, Y., JACOX, L. A., LITTLE, S. H. & KO, C. C. 2018. Orthodontic tooth movement: The biology and clinical implications. *Kaohsiung J Med Sci,* 34**,** 207-214.

41. LIU, P., CHENG, H., ROBERTS, T. M. & ZHAO, J. J. 2009. Targeting the phosphoinositide 3-kinase pathway in cancer. *Nat Rev Drug Discov,* 8**,** 627-44.

42. MARKHAM, A. 2019. Alpelisib: First Global Approval. *Drugs,* 79**,** 1249-1253.

43. MAYER, I. A., ABRAMSON, V. G., FORMISANO, L., BALKO, J. M., ESTRADA, M. V., SANDERS, M. E., JURIC, D., SOLIT, D., BERGER, M. F., WON, H. H., LI, Y., CANTLEY, L. C., WINER, E. & ARTEAGA, C. L. 2017. A Phase Ib Study of Alpelisib (BYL719), a PI3Kalpha-Specific Inhibitor, with Letrozole in ER+/HER2- Metastatic Breast Cancer. *Clin Cancer Res,* 23**,** 26-34.

44. MEGDANOVA-CHIPEVA, V. G., LAMARCA, A., BACKEN, A., MCNAMARA, M. G., BARRIUSO, J., SERGIEVA, S., GOCHEVA, L., MANSOOR, W., MANOHARAN, P. & VALLE, J. W. J. C. 2020. Systemic Treatment Selection for

Patients with Advanced Pancreatic Neuroendocrine Tumours (PanNETs). 12**,** 1988.

45. MOHAN, A. M., BEINDORFF, N. & BRENNER, W. 2021. Nuclear Medicine Imaging Procedures in Oncology. *Methods Mol Biol,* 2294**,** 297-323.

46. MOHAN, A. M., LUKAS, M., ALBRECHT, J., DORAU-RUTKE, V., KOZIOLEK, E. J., HUANG, K., PRASAD, S., BRENNER, W. & BEINDORFF, N. 2020. Relationship of Renal Function in Mice to Strain, Sex and 177Lutetium-Somatostatin Receptor Ligand Treatment. *Nuklearmedizin,* 59**,** 381-386.

47. MOHAN, A. M., PRASAD, S., SCHMITZ-PEIFFER, F., LANGE, C., LUKAS, M., KOZIOLEK, E. J., ALBRECHT, J., MESSROGHLI, D., STEIN, U., ILMER, M., WANG, K., SCHOBER, L., REUL, A., MAURER, J., FRIEMEL, J., WEBER, A., ZUELLIG, R. A., HANTEL, C., FRITSCH, R., REINCKE, M., PACAK, K., GROSSMAN, A. B., AUERNHAMMER, C. J., BEUSCHLEIN, F., BRENNER, W., BEINDORFF, N. & NOLTING, S. 2024. Impact of the PI3K-alpha inhibitor alpelisib on everolimus resistance and somatostatin receptor expression in an orthotopic pancreatic NEC xenograft mouse model. *Endocr Relat Cancer,* 31**,** ERC-23-0041.

48. NAGTEGAAL, I. D., ODZE, R. D., KLIMSTRA, D., PARADIS, V., RUGGE, M., SCHIRMACHER, P., WASHINGTON, K. M., CARNEIRO, F., CREE, I. A. & BOARD, W. H. O. C. O. T. E. 2020. The 2019 WHO classification of tumours of the digestive system. *Histopathology,* 76**,** 182-188.

49. NASWA, N., BAL, C., LATA, S., REDDY, R. & MALHOTRA, A. 2010. A comparison of 68Gallium-DOTA-TOC and 18F-FDG PET/CT in imaging of neuroendocrine tumors (NETs). *Journal of Nuclear Medicine,* 51**,** 405-405.

50. NOLTING, S., RENTSCH, J., FREITAG, H., DETJEN, K., BRIEST, F., MOBS, M., WEISSMANN, V., SIEGMUND, B., AUERNHAMMER, C. J., ARISTIZABAL PRADA, E. T., LAUSEKER, M., GROSSMAN, A., EXNER, S., FISCHER, C., GROTZINGER, C., SCHRADER, J., GRABOWSKI, P. & GROUP, G. N.-Z. S. 2017. The selective PI3Kalpha inhibitor BYL719 as a novel therapeutic option for

neuroendocrine tumors: Results from multiple cell line models. *PLoS One,* 12**,** e0182852.

51. NÖLTING, S., RENTSCH, J., FREITAG, H., DETJEN, K., BRIEST, F., MOBS, M., WEISSMANN, V., SIEGMUND, B., AUERNHAMMER, C. J., ARISTIZABAL PRADA, E. T., LAUSEKER, M., GROSSMAN, A., EXNER, S., FISCHER, C., GROTZINGER, C., SCHRADER, J., GRABOWSKI, P. & GROUP, G. N.-Z. S. 2017. The selective PI3Kalpha inhibitor BYL719 as a novel therapeutic option for neuroendocrine tumors: Results from multiple cell line models. *PLoS One,* 12**,** e0182852.

52. NUNNERY, S. E. & MAYER, I. A. 2019. Management of toxicity to isoform alpha-specific PI3K inhibitors. *Ann Oncol,* 30**,** x21-x26.

53. OHIRA, T., DE VIT, A. & DIBART, S. 2020. Strategic Use of Ultrasonic Frequencies for Targeted Bone Biomodification Following Piezoelectric Bone Surgery in Rats. Part II: Late Phase. *Int J Periodontics Restorative Dent,* 40**,** 591-600.

54. PAIELLA, S., LANDONI, L., TEBALDI, S., ZUFFANTE, M., SALGARELLO, M., CINGARLINI, S., D'ONOFRIO, M., PARISI, A., DEIRO, G., MANFRIN, E., BIANCHI, B., MONTAGNINI, G., CRINO, S. F., BASSI, C. & SALVIA, R. 2021. Dual-Tracer (68Ga-DOTATOC and 18F-FDG-)-PET/CT Scan and G1-G2 Nonfunctioning Pancreatic Neuroendocrine Tumors: A Single-Center Retrospective Evaluation of 124 Nonmetastatic Resected Cases. *Neuroendocrinology*.

55. PANAGIOTIDIS, E., ALSHAMMARI, A., MICHOPOULOU, S., SKOURA, E., NAIK, K., MARAGKOUDAKIS, E., MOHMADUVESH, M., AL-HARBI, M., BELDA, M., CAPLIN, M. E., TOUMPANAKIS, C. & BOMANJI, J. 2017. Comparison of the Impact of 68Ga-DOTATATE and 18F-FDG PET/CT on Clinical Management in Patients with Neuroendocrine Tumors. *J Nucl Med,* 58**,** 91-96.

56. PAPADOPOULOS, N., BEINDORFF, N., HOFFMANN, S., JOST-BRINKMANN, P. G. & PRAGER, T. M. 2021. Impact of piezocision on orthodontic tooth movement. *Korean J Orthod,* 51**,** 366-374.

57. PARGHANE, R. V., BHANDARE, M., CHAUDHARI, V., OSTWAL, V., RAMASWAMY, A., TALOLE, S., SHRIKHANDE, S. V. & BASU, S. 2021. Surgical Feasibility, Determinants, and Overall Efficacy of Neoadjuvant (177)Lu-DOTATATE PRRT for Locally Advanced Unresectable Gastroenteropancreatic Neuroendocrine Tumors. *J Nucl Med,* 62**,** 1558-1563.

58. PASSACANTILLI, I., CAPURSO, G., ARCHIBUGI, L., CALABRETTA, S., CALDAROLA, S., LORENI, F., DELLE FAVE, G. & SETTE, C. 2014. Combined therapy with RAD001 e BEZ235 overcomes resistance of PET immortalized cell lines to mTOR inhibition. *Oncotarget,* 5**,** 5381-91.

59. PAVEL, M. & DE HERDER, W. W. 2017. ENETS Consensus Guidelines for the Standard of Care in Neuroendocrine Tumors. *Neuroendocrinology,* 105**,** 193-195.

60. PAVEL, M., O'TOOLE, D., COSTA, F., CAPDEVILA, J., GROSS, D., KIANMANESH, R., KRENNING, E., KNIGGE, U., SALAZAR, R., PAPE, U. F., OBERG, K. & VIENNA CONSENSUS CONFERENCE, P. 2016. ENETS Consensus Guidelines Update for the Management of Distant Metastatic Disease of Intestinal, Pancreatic, Bronchial Neuroendocrine Neoplasms (NEN) and NEN of Unknown Primary Site. *Neuroendocrinology,* 103**,** 172-85.

61. PAVEL, M. E. & SERS, C. J. E.-R. C. 2016. WOMEN IN CANCER THEMATIC REVIEW: Systemic therapies in neuroendocrine tumors and novel approaches toward personalized medicine. 23**,** T135.

62. POGODA, P., PRIEMEL, M., SCHILLING, A. F., GEBAUER, M., CATALA-LEHNEN, P., BARVENCIK, F., BEIL, F. T., MUNCH, C., RUPPRECHT, M., MULDNER, C., RUEGER, J. M., SCHINKE, T. & AMLING, M. 2005. Mouse models in skeletal physiology and osteoporosis: experiences and data on 14,839 cases from the Hamburg Mouse Archives. *J Bone Miner Metab,* 23 Suppl**,** 97-102.

63. POPA, O., TABAN, S. M., PANTEA, S., PLOPEANU, A. D., BARNA, R. A., CORNIANU, M., PASCU, A. A. & DEMA, A. L. C. 2021. The new WHO classification of gastrointestinal neuroendocrine tumors and immunohistochemical expression of somatostatin receptor 2 and 5. *Exp Ther Med,* 22**,** 1179.

64. QI, J., KITAURA, H., SHEN, W. R., KISHIKAWA, A., OGAWA, S., OHORI, F., NOGUCHI, T., MARAHLEH, A., NARA, Y. & MIZOGUCHI, I. 2019. Establishment of an orthodontic retention mouse model and the effect of anti-c-Fms antibody on orthodontic relapse. *PLoS One,* 14**,** e0214260.

65. REN, Y., MALTHA, J. C. & KUIJPERS-JAGTMAN, A. M. 2004. The rat as a model for orthodontic tooth movement--a critical review and a proposed solution. *Eur J Orthod,* 26**,** 483-90.

66. RO, C., CHAI, W. X., YU, V. E. & YU, R. 2013. Pancreatic neuroendocrine tumors: biology, diagnosis, and treatment. *Chinese Journal of Cancer,* 32**,** 312-324.

67. ROSNER, M. H. & PERAZELLA, M. A. 2019. Acute kidney injury in the patient with cancer. *Kidney Res Clin Pract,* 38**,** 295-308.

68. ROWE, P., KOLLER, A. & SHARMA, S. 2023. Physiology, Bone Remodeling. *StatPearls.* Treasure Island (FL).

69. RUDISILE, S., GOSEWISCH, A., WENTER, V., UNTERRAINER, M., BONING, G., GILDEHAUS, F. J., FENDLER, W. P., AUERNHAMMER, C. J., SPITZWEG, C., BARTENSTEIN, P., TODICA, A. & ILHAN, H. 2019. Salvage PRRT with (177)Lu-DOTA-octreotate in extensively pretreated patients with metastatic neuroendocrine tumor (NET): dosimetry, toxicity, efficacy, and survival. *BMC Cancer,* 19**,** 788.

70. SANTONI, M., PANTANO, F., AMANTINI, C., NABISSI, M., CONTI, A., BURATTINI, L., ZOCCOLI, A., BERARDI, R., SANTONI, G., TONINI, G., SANTINI, D. & CASCINU, S. 2014. Emerging strategies to overcome the resistance to current mTOR inhibitors in renal cell carcinoma. *Biochim Biophys Acta,* 1845**,** 221-31.

71. SASSIER, M., DUGUE, A. E., CLARISSE, B., LESUEUR, P., AVRILLON, V., BIZIEUX-THAMINY, A., AULIAC, J. B., KALUZINSKI, L., TILLON, J., ROBINET, G., LE CAER, H., MONNET, I., MADROSZYK, A., BOZA, G., FALCHERO, L., FOURNEL, P., EGENOD, T., TOFFART, A. C., LEIBER, N., DO, P. & GERVAIS, R. 2015. Renal insufficiency is the leading cause of double maintenance (bevacizumab and pemetrexed) discontinuation for toxicity to advanced non-small cell lung cancer in real world setting. *Lung Cancer,* 89**,** 161-6.

72. STROSBERG, J., EL-HADDAD, G., WOLIN, E., HENDIFAR, A., YAO, J., CHASEN, B., MITTRA, E., KUNZ, P. L., KULKE, M. H., JACENE, H., BUSHNELL, D., O'DORISIO, T. M., BAUM, R. P., KULKARNI, H. R., CAPLIN, M., LEBTAHI, R., HOBDAY, T., DELPASSAND, E., VAN CUTSEM, E., BENSON, A., SRIRAJASKANTHAN, R., PAVEL, M., MORA, J., BERLIN, J., GRANDE, E., REED, N., SEREGNI, E., OBERG, K., LOPERA SIERRA, M., SANTORO, P., THEVENET, T., ERION, J. L., RUSZNIEWSKI, P., KWEKKEBOOM, D., KRENNING, E. & INVESTIGATORS, N.-T. 2017. Phase 3 Trial of (177)Lu-Dotatate for Midgut Neuroendocrine Tumors. *N Engl J Med,* 376**,** 125-135.

73. STROSBERG, J. R., CAPLIN, M. E., KUNZ, P. L., RUSZNIEWSKI, P. B., BODEI, L., HENDIFAR, A., MITTRA, E., WOLIN, E. M., YAO, J. C., PAVEL, M. E., GRANDE, E., VAN CUTSEM, E., SEREGNI, E., DUARTE, H., GERICKE, G., BARTALOTTA, A., MARIANI, M. F., DEMANGE, A., MUTEVELIC, S., KRENNING, E. P. & INVESTIGATORS, N.-. 2021. (177)Lu-Dotatate plus long-acting octreotide versus highdose long-acting octreotide in patients with midgut neuroendocrine tumours (NETTER-1): final overall survival and long-term safety results from an open-label, randomised, controlled, phase 3 trial. *Lancet Oncol,* 22**,** 1752-1763.

74. TADDEI, S. R., MOURA, A. P., ANDRADE, I., JR., GARLET, G. P., GARLET, T. P., TEIXEIRA, M. M. & DA SILVA, T. A. 2012. Experimental model of tooth movement in mice: a standardized protocol for studying bone remodeling under compression and tensile strains. *J Biomech,* 45**,** 2729-35.

75. TREGLIA, G., CASTALDI, P., RINDI, G., GIORDANO, A. & RUFINI, V. 2012. Diagnostic performance of Gallium-68 somatostatin receptor PET and PET/CT in

patients with thoracic and gastroenteropancreatic neuroendocrine tumours: a meta-analysis. *Endocrine,* 42**,** 80-7.

76. UPADHYAY, B., MO, J., BEADSMOORE, C., MARSHALL, T., TOMS, A. & BUSCOMBE, J. 2017. Technetium-99m Methylene Diphosphonate Single-photon Emission Computed Tomography/Computed Tomography of the Foot and Ankle. *World J Nucl Med,* 16**,** 88-100.

77. VANDAMME, T., BEYENS, M., DE BEECK, K. O., DOGAN, F., VAN KOETSVELD, P. M., PAUWELS, P., MORTIER, G., VANGESTEL, C., DE HERDER, W., VAN CAMP, G., PEETERS, M. & HOFLAND, L. J. 2016. Long-term acquired everolimus resistance in pancreatic neuroendocrine tumours can be overcome with novel PI3K-AKT-mTOR inhibitors. *Br J Cancer,* 114**,** 650-8.

78. VEGT, E., DE JONG, M., WETZELS, J. F., MASEREEUW, R., MELIS, M., OYEN, W. J., GOTTHARDT, M. & BOERMAN, O. C. 2010. Renal toxicity of radiolabeled peptides and antibody fragments: mechanisms, impact on radionuclide therapy, and strategies for prevention. *J Nucl Med,* 51**,** 1049-58.

79. VEGT, E., MELIS, M., EEK, A., DE VISSER, M., BROM, M., OYEN, W. J., GOTTHARDT, M., DE JONG, M. & BOERMAN, O. C. 2011. Renal uptake of different radiolabelled peptides is mediated by megalin: SPECT and biodistribution studies in megalin-deficient mice. *Eur J Nucl Med Mol Imaging,* 38**,** 623-32.

80. WERNER, R. A., BEYKAN, S., HIGUCHI, T., LUCKERATH, K., WEICH, A., SCHEURLEN, M., BLUEMEL, C., HERRMANN, K., BUCK, A. K., LASSMANN, M., LAPA, C. & HANSCHEID, H. 2016. The impact of 177Lu-octreotide therapy on 99mTc-MAG3 clearance is not predictive for late nephropathy. *Oncotarget,* 7**,** 41233-41241.

81. YANG, J., KAN, Y., GE, B. H., YUAN, L., LI, C. & ZHAO, W. 2014. Diagnostic role of Gallium-68 DOTATOC and Gallium-68 DOTATATE PET in patients with neuroendocrine tumors: a meta-analysis. *Acta Radiol,* 55**,** 389-98.

82. YAO, J. C., FAZIO, N., SINGH, S., BUZZONI, R., CARNAGHI, C., WOLIN, E., TOMASEK, J., RADERER, M., LAHNER, H., VOI, M., PACAUD, L. B., ROUYRRE,

N., SACHS, C., VALLE, J. W., FAVE, G. D., VAN CUTSEM, E., TESSELAAR, M., SHIMADA, Y., OH, D. Y., STROSBERG, J., KULKE, M. H., PAVEL, M. E. & RAD001 IN ADVANCED NEUROENDOCRINE TUMOURS, F. T. S. G. 2016. Everolimus for the treatment of advanced, non-functional neuroendocrine tumours of the lung or gastrointestinal tract (RADIANT-4): a randomised, placebo-controlled, phase 3 study. *Lancet,* 387**,** 968-977.

83. YOSHIDA, S., KAWAI, H., EGUCHI, T., SUKEGAWA, S., OO, M. W., ANQI, C., TAKABATAKE, K., NAKANO, K., OKAMOTO, K. & NAGATSUKA, H. 2019. Tumor Angiogenic Inhibition Triggered Necrosis (TAITN) in Oral Cancer. *Cells,* 8.

84. ZHANG, J., KULKARNI, H., SINGH, A., NIEPSCH, K., SCHUCHARDT, C. & BAUM, R. 2019. Long-term nephrotoxicity after peptide receptor radionuclide therapy (PRRT): myth or reality? : Soc Nuclear Med.

85. ZHANG, P., YU, J., LI, J., SHEN, L., LI, N., ZHU, H., ZHAI, S., ZHANG, Y., YANG, Z. & LU, M. 2018. Clinical and Prognostic Value of PET/CT Imaging with Combination of (68)Ga-DOTATATE and (18)F-FDG in Gastroenteropancreatic Neuroendocrine Neoplasms. *Contrast Media Mol Imaging,* 2018**,** 2340389.

86. ZHOU, Z., WANG, Z., ZHANG, B., WU, Y., LI, G. & WANG, Z. 2021. Comparison of 68Ga-DOTANOC and 18F-FDG PET-CT Scans in the Evaluation of Primary Tumors and Lymph Node Metastasis in Patients With Rectal Neuroendocrine Tumors. *Front Endocrinol (Lausanne),* 12**,** 727327.

Statutory Declaration

“I, [**Ajay-Mohan, Mohan**], by personally signing this document in lieu of an oath, hereby affirm that I prepared the submitted dissertation on the topic [[PET/CT and SPECT/CT for monitoring treatment response and treatment related morbidities in various oncological and non-oncological rodent models & PET/CT und SPECT/CT zur Erfassung des Therapieansprechens sowie von therapiebedingten Veränderungen in verschiedenen on-kologischen und nicht-onkologischen Nagetiermodellen], independently and without the support of third parties, and that I used no other sources and aids than those stated.
All parts which are based on the publications or presentations of other authors, either in letter or in spirit, are specified as such in accordance with the citing guidelines. The sections on methodology (in particular regarding practical work, laboratory regulations, statistical processing) and results (in particular regarding figures, charts and tables) are exclusively my responsibility.

Furthermore, I declare that I have correctly marked all of the data, the analyses, and the conclusions generated from data obtained in collaboration with other persons, and that I have correctly marked my own contribution and the contributions of other persons (cf. declaration of contribution). I have correctly marked all texts or parts of texts that were generated in collaboration with other persons.

My contributions to any publications to this dissertation correspond to those stated in the below joint declaration made together with the supervisor. All publications created within the scope of the dissertation comply with the guidelines of the ICMJE (International Committee of Medical Journal Editors; http://www.icmje.org) on authorship. In addition, I declare that I shall comply with the regulations of Charité – Universitätsmedizin Berlin on ensuring good scientific practice.

I declare that I have not yet submitted this dissertation in identical or similar form to another Faculty.

The significance of this statutory declaration and the consequences of a false statutory declaration under criminal law (Sections 156, 161 of the German Criminal Code) are known to me.”

Date: 27.02.2024 Signature

Declaration of your own contribution to the publications

Ajay-Mohan Mohan contributed the following to the below listed publications:

Publication 1: [**Ajay-Mohan Mohan**, Sonal Prasad, Fabian Schmitz-Peiffer, Catharina Lange, Mathias Lukas, Eva J. Koziolek, Jakob Albrecht , Daniel Messroghli, Ulrike Stein, Matthias Ilmer, Katharina Wang, Laura Schober, Astrid Reul, Julian Maurer, Juliane Friemel, Achim Weber, Richard Zuellig, Constanze Hantel, Ralph Fritsch, Martin Reincke, Karel Pacak, Ashley Grossman, Christoph Josef Auernhammer, Felix Beuschlein, Winfried Brenner Nicola Beindorff, Svenja Nölting], [Impact of the PI3Kalpha inhibitor alpelisib on everolimus resistance and somatostatin receptor expression in an orthotopic pancreatic NEC xenograft mouse model], [Endocrine Related Cancer], [2024]
Contribution (please set out in detail):

1. Conduction of the preparatory experiments. This has resulted in:
    a. The imaging protocols ultimately used (Material and Methods) and Table 1, Table 2, Table 3 and Publication 1 by Mohan et al.
    b. The oral chemotherapeutic regimen (material and methods)
2. The practical performance of all cell culture procedures (material and methods) and the majority of imaging.
3. Evaluation and interpretation of the image data as well as the performance of descriptive statistics. This resulted in:
    a. Figure 1 and 2
    b. Table 1 and 2
4. Manuscript preparation and submission for publication

Publication 2: [**Ajay-Mohan Mohan**, Mathias Lukas, Jakob Albrecht, Viktoria Dorau-Rutke, Eva J. Koziolek, Kai Huang, Sonal Prasad, Winfried Brenner, Nicola Beindorff], [Relationship of Renal Function in Mice to Strain, Sex and 177Lutetium-Somatostatin Receptor Ligand Treatment], [Nuklearmedizin], [2020]
Contribution (please set out in detail):

1. Evaluation and interpretation of the image data.
   This resulted in:
    a. Figure 1 and 2
    b. Table 1
2. Manuscript preparation for publication

Publication 3: [Nicola Beindorff, Nikolaos Papadopoulos, Stefan Hoffmann, **Ajay-Mohan Mohan**, Mathias Lukas, Winfried Brenner, Paul-Georg Jost-Brinkmann, Thomas Präger], [Nuklearmedizin], [2022]
Contribution (please set out in detail):

1. Manuscript preparation for publication

_____

Signature, date and stamp of first supervising university professor / lecturer

_____

Signature of doctoral candidate

Printing copy(s) of the publication(s)

1. Mohan, A. M., Prasad, S., Schmitz-Peiffer, F., Lange, C., Lukas, M., Koziolek, E. J., Albrecht, J., Messroghli, D., Stein, U., Ilmer, M., Wang, K., Schober, L., Reul, A., Maurer, J., Friemel, J., Weber, A., Zuellig, R. A., Hantel, C., Fritsch, R., Reincke, M., … Nölting, S. (2023). Impact of the PI3K-alpha inhibitor alpelisib on everolimus resistance and somatostatin receptor expression in an orthotopic pancreatic NEC xenograft mouse model. *Endocrine-related cancer*, *31*(1), e230041. https://doi.org/10.1530/ERC-23-0041
2. Mohan, A. M., Lukas, M., Albrecht, J., Dorau-Rutke, V., Koziolek, E. J., Huang, K., Prasad, S., Brenner, W., & Beindorff, N. (2020). Relationship of Renal Function in Mice to Strain, Sex and 177Lutetium-Somatostatin Receptor Ligand Treatment. Nierenfunktion bei Mäusen in Abhängigkeit von Stamm, Geschlecht und 177Lutetium-Somatostatin-Rezeptor-Liganden-Therapie. *Nuklearmedizin. Nuclear medicine*, *59*(5), 381–386. https://doi.org/10.1055/a-1103-1661
3. Beindorff, N., Papadopoulos, N., Hoffmann, S., Mohan, A. M., Lukas, M., Brenner, W., Jost-Brinkmann, P. G., & Präger, T. (2022). Monitoring orthodontic tooth movement in rats after piezocision by bone scintigraphy. Skelettszintigraphische Untersuchungen kieferorthopädischer Zahnbewegungen bei Ratten nach Piezotomie. *Nuklearmedizin. Nuclear medicine*, *61*(5), 402–409. https://doi.org/10.1055/a-1816-6825

Curriculum Vitae

“My curriculum vitae does not appear in the electronic version of my paper for reasons of data protection”

Publication list

ORIGINAL ARTICLES

1. Schmitz-Peiffer F, Lukas M, **Mohan AM**, Albrecht J, Aschenbach JR, Brenner W, Beindorff N. Effects of isoflurane anaesthesia depth and duration on renal function measured with [^{99m}Tc]Tc-mercaptoacetyltriglycine SPECT in mice. EJNMMI Res 2024 Jan 5;14(1):4. doi: 10.1186/s13550-023-01065-3. (2023) IF: 3.2

2. **Mohan AM**, Prasad S, Schmitz-Peiffer F, Lange C, Lukas M, Koziolek EJ, Albrecht J, Messroghli D, Stein U, Ilmer M, Wang K. Impact of the PI3K-alpha inhibitor alpelisib on everolimus resistance and somatostatin receptor expression in an orthotopic pancreatic NEC xenograft mouse model. Endocrine-related cancer. 2023 Nov 30;31(1):e230041.doi: 10.1530/ERC-23-0041.IF: 3.9

3. Beindorff N, Papadopoulos N, Hoffmann S, **Mohan AM**, Lukas M, Brenner W, Jost-Brinkmann PG, Präger T. Monitoring orthodontic tooth movement in rats after piezocision by bone scintigraphy. Nuklearmedizin. 2022 Oct;61(5):402-409. doi: 10.1055/a-1816-6825 IF: 1.5

4. Zboralski D, Hoehne A, Bredenbeck A, Schumann A, Nguyen M, Schneider E, Ungewiss J, Paschke M, Haase C, von Hacht JL, Kwan T, Lin KK, Lenore J, Harding TC, Xiao J, Simmons AD, **Mohan AM**, Beindorff N, Reineke U, Smerling C, Osterkamp F. Preclinical evaluation of FAP-2286 for fibroblast activation protein targeted radionuclide imaging and therapy. Eur J Nucl Med Mol Imaging. 2022 Sep;49:3651-3667. doi: 10.1007/s00259-022-05842-5 IF: 9.1

5. **Mohan AM**, Lukas M, Albrecht J, Dorau-Rutke V, Koziolek EJ, Huang K, Prasad S, Brenner W, Beindorff N. Relationship of Renal Function in Mice to Strain, Sex and 177Lutetium-Somatostatin Receptor Ligand Treatment. Nuklearmedizin. 2020 Sep;59(5):381-386. doi: 10.1055/a-1103-1661 IF: 1.5

ABSTRACTS

1. Schmitz-Peiffer F, Lukas M, **Mohan AM**, Brenner W, Beindorff N. Effects of single and multiple mouse beds on renal function measured with Tc-99m-Mercaptoacetyltriglycine SPECT in isoflurane anaesthesia. Nuklearmedizin 62:153-154 (2023)

2. **Mohan A**, Prasad S, Schmitz-Peiffer F, Lange C, Lukas M, Koziolek EJ, Pacak K, Ilmer M, Grossman A, Wang K, Reul A, Maurer J, Schober L, Friemel J, Reincke M, Auernhammer CJ, Beuschlein F, Brenner W, Nölting S, Beindorff N. Effects of PI3kα inhibitor BYL719 on overcoming everolimus resistance and inducing re-expression of somatostatin receptors in an everolimus-resistant orthotopic pancreatic NET xenograft mouse model. Eur J Nucl Med Mol Imaging.2022;49 (Suppl 1): S329

3. Zboralski D, Osterkamp F, Simmons AD, Bredenbeck A, Schumann A, Paschke M, Beindorff N, **Mohan AM**, Nguyen M, Xiao J, Harding TC. 571P Preclinical evaluation of FAP-2286, a peptide-targeted radionuclide therapy (PTRT) to fibroblast activation protein alpha (FAP). Annals of Oncology. 2020 Sep 1;31:S488.

4. **Mohan AM**, Lukas M, Albrecht J, Huang K, Brenner W, Beindorff N. Kidney function in mice with respect to strain, sex and Lu-177-DOTATOC treatment. Nuklearmedizin-NuclearMedicine. 2020 Apr;59(02):P127.

BOOK CHAPTERS

1. Prasad S, **Mohan AM**, Huang K, Prasad V. Nuclear medicine therapy of lung cancer, breast cancer and colorectal cancer. InNuclear Medicine and Molecular Imaging: Volume 1-4 2022 Jan 1 (pp. 278-287). (Elsevier)

2. **Mohan AM**, Beindorff N, Brenner W. Nuclear Medicine Imaging Procedures in Oncology. Methods Mol Biol. 2021;2294:297-323. doi: 10.1007/978-1-0716-1350-4_21. PMID: 33742410. (Springer)

Acknowledgments

I wholeheartedly thank my supervisors Professor Dr. med. Winfried Brenner and Dr. med. vet. Nicola Beindorff for their constant responsiveness and support as well as their constructive criticism and encouragement during the whole project period. Furthermore, my sincere thanks goes to Dr. Sonal Prasad for helping me out with cell culture assays and with radiolabelling of various PET tracers. I would also like to thank Professor Svenja Nölting for giving me this opportunity to work on the NET project. Alongside I would also like to thank Prof. Baljinder Singh from India for bridging the contact with Professor Winfried Brenner for my Ph.D. dissertation.

Furthermore, my extraordinary thanks go to my supervisor Professor Dr. Ulrike Stein for providing the constant encouragement all throughout this time and all the other authors of the project for the friendly and cooperative collaboration.

I extend my gratitude towards German Academic Exchange Service (DAAD) for financially supporting me during my research stay here in Germany. I also extend my sincere thanks to Nachwuchs Committee from Charité - Universitätsmedizin Berlin for providing me with Ruth-Jeschke Scholarship to aid in finalizing my thesis. I would also like to thank my graduate school “Berlin School of Integrative Oncology (BSIO)” for allowing me to carry out my duties in the professional capacity of a doctoral student.

Last but not least, I would like to thank my family and friends for their emotional support during the intensive working time on the dissertation and also in helping me to withstand the tough COVID times.